Azimuth-Altitude Dual Axis Solar Tracker

December 16, 2010

A Master Qualifying Project: submitted to the faculty of
WORCESTER POLYTECHNIC INSTITUTE
In fulfillment of the
Degree of Bachelor of Science

Submitted by:

Adrian Catarius
acatarius@wpi.edu

Mario Christiner
mariopchristiner@wpi.edu

Faculty Advisor:

Professor Alexander Emanuel

Abstract

People in underprivileged countries could benefit from the use of a solar distributed generation system. To provide an efficient solar distributed generation system, a scaled down dual-axis solar tracker was designed, built and tested. At maximum, the solar tracker was perpendicular to the light source by 1.5 degrees. The built system had a calculated annual energy gain of 48.982% compared to an immobile solar panel. Compared to a single axis tracker, the dual-axis tracker had an annual energy gain of 36.504%.

Acknowledgements

We would like to thank the various electrical engineering faculty members at Worcester Polytechnic Institute who helped create this project; Tom Agelotti, Patrick Morrison, and Dr. James O’Rourke.

Finally, we thank Professor Alexander Emanuel for all his patience and everlasting help.

Table of Contents

Figures

Tables

List of Acronyms

AADAT: Azimuth-Altitude Dual Axis Tracker

ADC: Analog to Digital Converter

BJT: Bipolar Junction Transistor

CFC: Chlorofluorocarbon

CMOS: Complementary Metal-Oxide-Semiconductor

DC: Direct Current

DG: Distributed Generation

EMF: Electromagnetic Field

HSAT: Horizontal Single Axis Tracker

LED: Light-Emitting Diode

MOSFET: Metal-Oxide-Semiconductor Field-Effect Transistor

MPPT: Maximum Power Peak Tracker

PASAT: Polar Aligned Single Axis Tracker

PCB: Printed Circuit Board

PIC: Programmable Interface Controller

PSPICE: Personal Simulation with Integrated Circuit Emphasis

PV: Photovoltaic

PWM: Pulse Width Modulation

SPST: Single Pole, Single Throw

TSAT: Tilted Single Axis Tracker

TTDAT: Tip-Tilt Dual Axis Tracker

VSAT: Vertical Single Axis Tracker

1 Introduction: The Need for Electricity in Underprivileged Countries and a Possible Solution

Not all countries possess all the commodities that are available to humanity. These so called underprivileged countries lack amenities such as; abundant food, clean water, medicine, wealth, education, and a healthy environment. The World Bank and other institutions believe that the lack of access to clean and efficient energy services is a factor involved in underprivileged countries from gaining more resources associated with higher living quality, such as wealth [1]. There are a few new forms of advanced energy, but electricity has been proven to be one of the cleanliest and most efficient forms [1].

One possible solution to unreliable or nonexistent central electricity distribution systems is to have distributed generation system (DG). A distributed generation system is characterized by the fact that the electricity is produced locally rather than externally. DG is often used in underprivileged countries; however, usually in the form of small generators that run on different types of fossil fuels. The use of renewable types of DG is preferable, since they provide a more sustainable and healthier environment. The most common DG options include; solar, wind, and thermal. [2]

In comparing the various forms of renewable DG, five factors must be considered: location, ease of installation, reliability, capacity, and cost. Thermal power is a location dependent, high cost option whereas wind has a lower cost but is unreliable due to changing wind conditions and requires regular mechanical maintenance [3]. Solar power has a relatively lower cost, easy to install and maintain, and for underprivileged countries near the equator, ideal for the location [3].

However the problem with solar power is that it is directly dependent on light intensity. To produce the maximum amount of energy, a solar panel must be perpendicular to the light source [4]. Because the sun moves both throughout the day as well as throughout the year, a solar panel must be able to follow the sun's movement to produce the maximum possible power. The solution is to use a tracking system that maintains the panel's orthogonal position with the light source. There are many tracking system designs available including passive and active systems with one or two axes of freedom [5].

The goal of our project was to design an active, dual axis, solar tracker that will have a minimum allowable error of 10° and also be economically feasible to market towards underprivileged countries. We started by examining the prior work done in solar tracking methods to determine our course of action. From there we designed and tested several mechanical and electrical options and chose the ones with the most desirable characteristics. Finally, we built our final tracking system, tested and compared it to ensure that we met our original goal.

2 Background: Solar Technology

As mentioned above in the introduction, the use of a tracking system greatly improves the power gain from solar radiation. This background goes into further detail on the operation of solar cells and the reason tracking is needed. The different tracking technologies are also described and how they compare to one another.

2.1 Solar Power Fundamentals

A fundamental understanding of how a photovoltaic panel works is essential in producing a highly efficient solar system. Solar panels are formed out of solar cells that are connected in parallel or series. When connected in series, there is an increase in the overall voltage, connected in parallel increases the overall current. Each individual solar cell is typically made out of crystalline silicon, although other types such as ribbon and thin-film silicone are gaining popularity.

PV cells consist of layered silicon that is doped with different elements to form a p-n junction. The p-type side will contain extra holes or positive charges. The n-type side will contain extra electrons or negative charges. This difference of charge forms a region that is charge neutral and acts as a sort of barrier. When the p-n junction is exposed to light, photons with the correct frequency will form an extra electron/hole pair. However, since the p-n junction creates a potential difference, the electrons can’t jump to the other side only the holes can. Thus, the electrons must exit through the metal connector and flow through the load, to the connector on the other side of the junction. [4] [6]

Because the PV cells generate a current, cells/panels can be modeled as DC current sources. The amount of current a PV panel produces has a direct correlation with the intensity of light the panel is absorbing. Below is a simple drawing of the system:

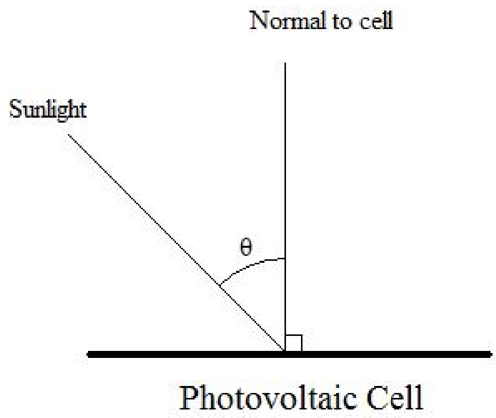

Figure 1: Angle of Incidence to Solar Cell (Adrian, 2010)

The normal to the cell is perpendicular to the cell's exposed face. The sunlight comes in and strikes the panel at an angle. The angle of the sunlight to the normal is the angle of incidence (θ). Assuming the sunlight is staying at a constant intensity (λ) the available sunlight to the solar cell for power generation (W) can be calculated as:

$$W = A \lambda \cos(\theta)$$

Here, A represents some limiting conversion factor in the design of the panel because they cannot convert 100% of the sunlight absorbed into electrical energy. By this calculation, the maximum power generated will be when the sunlight is hitting the PV cell along its normal and no power will be generated when the sunlight is perpendicular to the normal. With a fixed solar panel, there is significant power lost during the day because the panel is not kept perpendicular to the sun's rays. A tracking system can keep the angle of incidence within a certain margin and would be able to maximize the power generated. Mousazadeh et al. calculated the amount of power gained by tracking can come close to an ideal 57% difference [5]

2.2 Existing Tracking Technology

As mentioned in the previous sub-section (2.1) the absorption of light by a PV panel is dependent on its angular position to the sun. A PV panel must be perpendicular to the sun for maximum solar absorption, which is done by using a tracking system. Multiple tracking systems exist, which vary in reliability, accuracy, cost, and other factors. A tracking system must be chosen wisely to ensure that the tracking method increases the power gained instead of decreasing it.

2.2.1 Immobile Versus Mobile

Different power applications require different tracking systems. For certain applications a tracking system is too costly and will decrease the max power that is gained from the solar panel. Due to the fact that the earth rotates on its axis and orbits around the sun, if a PV cell/panel is immobile, the absorption efficiency will be significantly less at certain times of the day and year. The use of a tracking system to keep the PV cell/panel perpendicular to the sun can boost the collected energy by 10 - 100% depending on the circumstances [5].

If a tracking system is not used, the solar panel should still be oriented in the optimum position. The panel needs to be placed where no shadow will fall on it at any time of the day. Additionally, the best tilt angle should be determined based on the geographical location of the panel. As a general guideline for the northern hemisphere, the PV panel should be placed at a tilt angle equal to the latitude of the site and facing south [7]. However, for a more accurate position and tilt angel a theoretical model of the suns iridescence for the duration of a year is created and the angel and position is matched to the model.

Using one axis of tracking can provide a significant power gain to the system. Wikipedia claims that one axis trackers are placed into the following classifications: horizontal single axis tracker (HSAT), vertical single axis tracker (VSAT), tilted single axis tracker (TSAT), and polar aligned single axis tracker (PASAT). However, these terms don’t seem to be used in most articles discussing tracking methods. One article did mention that a TSAT at a tilt angle of 5° increases the annual collection radiation by 10% compared to a HSAT, a HSAT increases the annual collection radiation by 15% to a VSAT, and finally a PASAT increases the annual collection radiation by 10% over a HSAT [5]. Thus for one axis a PASAT or TSAT configuration would collect the most solar radiation. A few of these tracker types are shown in Figure 2.

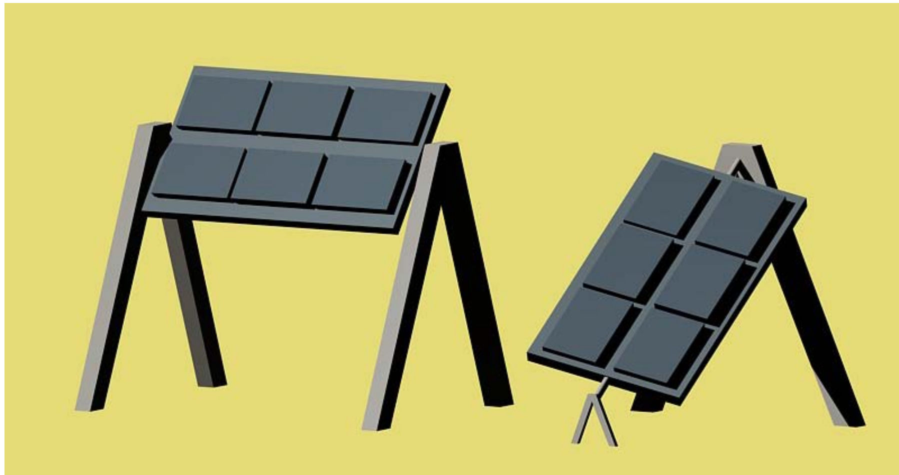

Figure 2: Different One Axis Trackers from Left to Right: HSAT and PASAT

For an additional power gain a dual-axis tracking system can be used. The percent gain from going from a PSAT to a dual-axis system is small [5], but as long as the system doesn't use more power than gained, it still helps. Again Wikipedia mentions two classifications for dual axis trackers: Tip-Tilt Dual Axis Tracker (TTDAT) and Azimuth-Altitude Dual Axis Tracker (AADAT). The difference between the two types is the orientation of the primary axis in relation to the ground. TTDAT's have the primary axis horizontal to the ground and AADAT's have theirs vertical. The azimuth/altitude method seems to be largely used, based on its reference in multiple research articles on tracking. [5]. In the article by Sefa et al. the following was stated; "The results indicated that increases of electrical power gains up to 43.87% for the two axes, 37.53% for the east–west, 34.43% for the vertical and 15.69% for the north–south tracking, as compared with the fixed surface inclined 32 to the south in Amman" [8]. A prototype AADAT was made in this project and a picture of it can be seen in Figure 6.

2.2.2 Passive Tracking Systems

One possible option for tracking is a chemical/mechanical system. This system uses the idea of thermal expansion of materials as a method for tracking. Typically a chlorofluorocarbon (CFC) or a type of shape memory alloy is placed on either side of the solar panel. When the panel is perpendicular with the sun, the two sides are at equilibrium. Once the sun moves, one side is heated and causes one side to expand and the other to contract, causing the solar panel to rotate. A passive system has the potential to increase efficiency by 23%. These systems are far cheaper than active systems, but according to Mousazadeh et al., are not commercially popular [5].

2.2.3 Active Tracking Systems

There are three main types of active tracker systems: auxiliary bifacial solar cell system, electro-optical system, and microprocessor/computer system.

Auxiliary bifacial solar cell systems are the simplest of the four active systems. A bifacial auxiliary solar cell (sensor cell) is fixed to the rotary axle of the tracker and is placed perpendicular to the main bifacial solar panel array. The sensor cell is connected directly to a motor, usually a DC electromotor. When the sun moves, the angle of incidence increases on the sensor cell, which eventually produces enough power to move the motor and the solar panel array. The example by Poulek and Libra claimed their system was able to collect 95% of the energy with a ± 5° tolerance. [9] This example can be seen in Figure 3.

Figure 3: Auxiliary Bifacial Solar Tracker

The electro-optical system is also another relatively simple system. Typically two photoresistors or PV cells are used as sensors for one-axis systems. These sensors are positioned near one another and have a divider, a tilted mount at a calculated angle, or use a collimator to create a useful current and/or voltage difference between the two sensors. These different setups are seen in Figure 4.

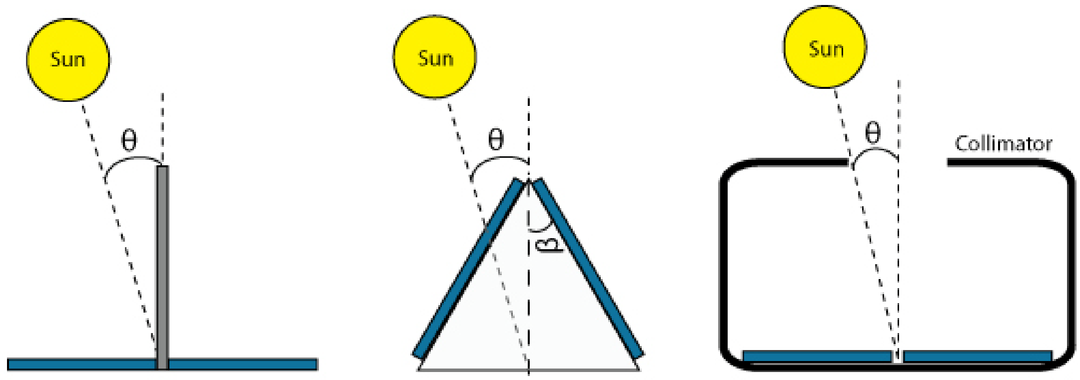

Figure 4: Tracker Sensor Setups from Left to Right: Divider, Tilted Mount, and Collimator

A combination of resistors, capacitors, amplifiers, logic gates, diodes, and transistors are used to form a comparison and driver circuit. The output of the comparing circuit powers a driver circuit, which in turn powers a motor and changes direction according to which sensor receives a higher amount of illumination. This orients the solar panel to be perpendicular to the sun. [5]

Microprocessor and computer systems make up the last type of system. They are sometimes classified into two different groups, but essentially they are quite similar. The main difference to the first two mentioned systems is microprocessor/computer systems use algorithms to determine the position of the sun instead of using sensors. Typically, microprocessor/computer systems only use sensors to reduce error or calibrate the system. Some microprocessor/computer systems even use a current maximization routine for error correction instead. In many systems a cheap microprocessor such as a Programmable Interface Controller (PIC) will have the algorithm for tracking, while information is fed to a computer, for analysis purposes. In Roth et al. the microcontroller has two primary modes, clock mode and sun mode. The clock mode calculates the position of the sun and makes any modification to the algorithm based on the solar error sensors. In the sun mode, the algorithm actively positions the solar panels. If the solar intensity decreases below a set value, the clock mode is activated. This variety of modes helps in better positioning and therefore a higher gain. [10]

3 System Design

The purpose of a solar tracker is to accurately determine the position of the sun. This enables solar panels interfaced to the tracker to obtain the maximum solar radiation. With this particular solar tracker a closed-loop system was made consisting of an electrical system and a mechanical system. The overall block-diagram can be seen in Figure 5.

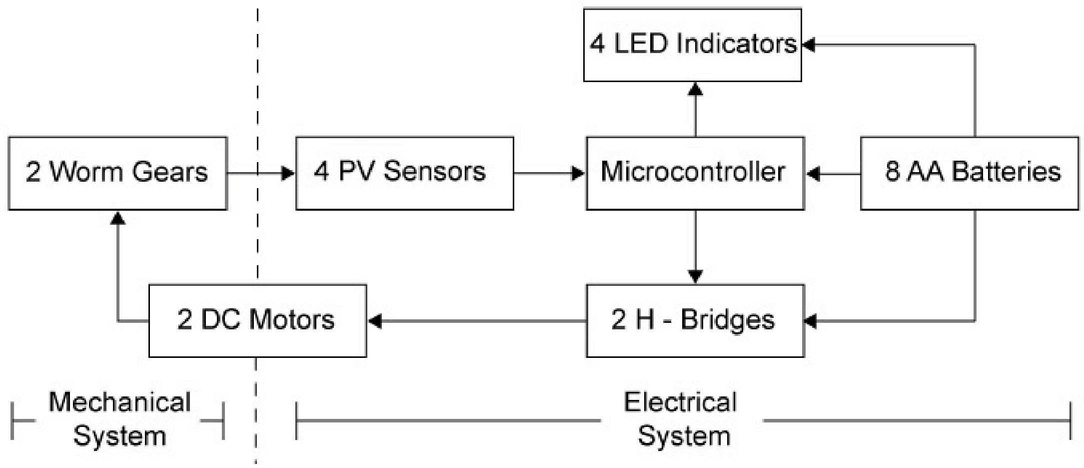

Figure 5: Block Diagram of Overall System

The electrical system consists of four PV sensors which provide feedback to a microcontroller. This microcontroller processes the sensor input and provides output to two H-Bridges and four LED indicators. The entire electrical system is powered by a 12V source, which consists of 8 AA batteries. The H-bridge controls the two DC motors, which are also part of the mechanical system. The mechanical system also contains two worm gear assemblies that adjust the PV sensors.

Initially an analog system was considered, in which a comparator circuit functioned as the central processor. A simple wooden prototype was built first to allow for testing of the PV sensors and DC motors. These tests were used to form an overall system simulation. In the process of testing it was determined that a microprocessor would be used instead of the comparator circuit, due to the improved efficiency. As the final step an acrylic prototype was constructed, as seen in Figure 6.

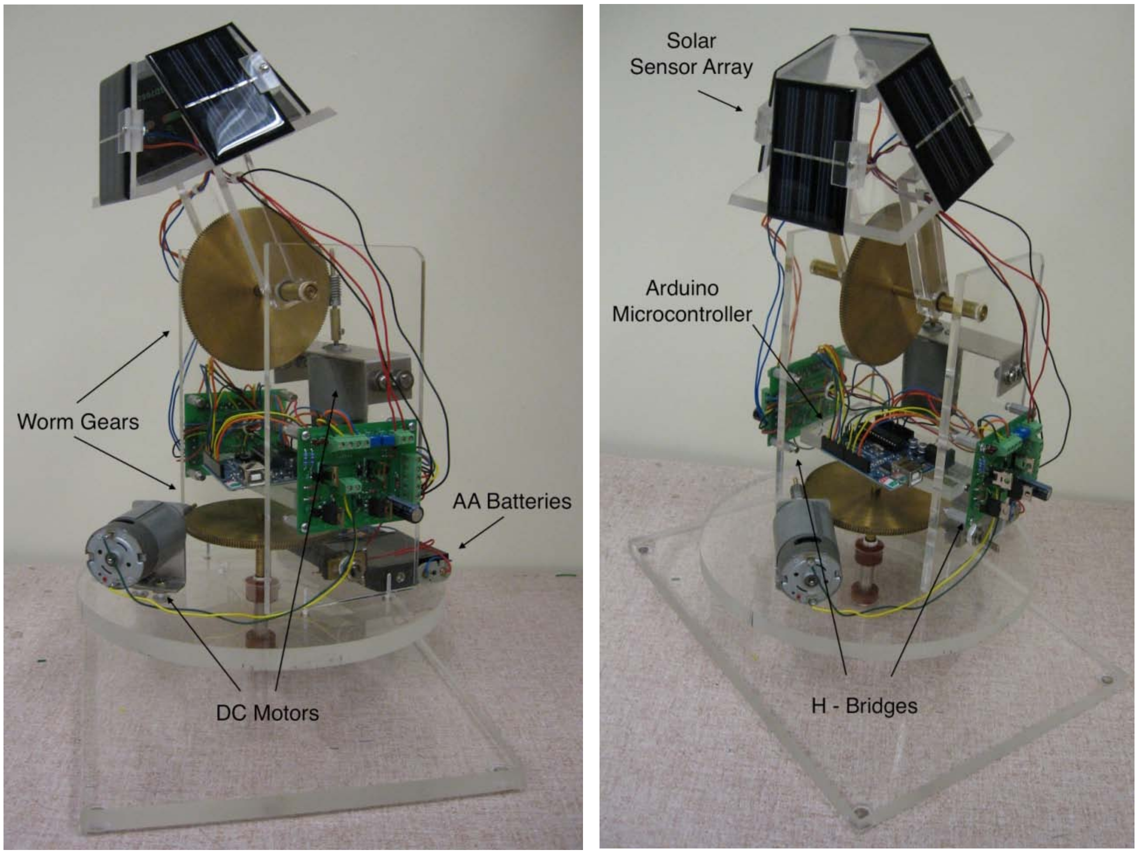

Figure 6: Final Solar Tracker Prototype

3.1 Mechanical System

As mentioned earlier, two separate prototypes were built and modified. The first prototype was constructed mainly from wood, with a few metal pieces used as shafts and bearings. The wooden prototype used a DC motor and a rubber belt to drive the system, then it was modified with a 50:1 worm gear drive. Finally, the acrylic prototype was built and was driven by a 180:1 worm gear drive. For each prototype the azimuth axis was designed and modified first, followed shortly by the altitude axis.

3.1.1 Motor

Two identical 12 V DC motors were donated to this project by Professor James O'Rourke. Unfortunately, these motors were surplus and had no known part number or documentation. Testing was required to find the resistance (R), inductance (L), and back electromagnetic field (EMF) constant k of the motor. These values were required in order to setup an accurate simulation according to the equations for a DC motor. The equation for the voltage across the motor is given as:

$$V = Ri + \frac{\partial i}{\partial t} L + k\omega$$

The mechanical equation for torque produced by the motor consists of constants for the inertia J, and damping factor D and the opposing torque T_O:

$$T = ki = D\omega + \frac{\partial \omega}{\partial t} J + T_O$$

Measuring for these values would allow an accurate simulation for the motor to calculate power requirements.

To get a value for the resistance of the motor, the voltage and current were measured while the motor was not spinning and the position of the shaft was altered. The resistance could be calculated using Ohm's Law, V = IR. The circuit used had two multimeters, one as a current meter and one as a voltage meter, with the motor connected through the ammeter straight to a variable DC power supply:

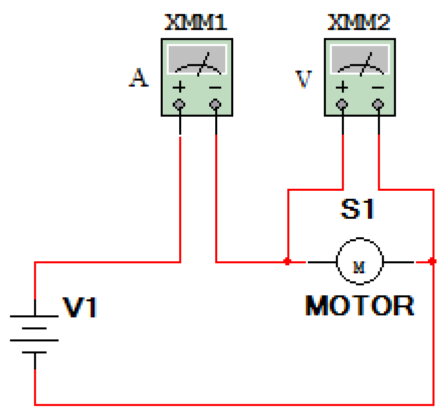

Figure 7: DC Motor Resistance Test Circuit

Because the motor had several poles where the shaft would try to settle in to, the shaft was moved slightly for each measurement so that an average value could be found. Table 1 shows the result of these measurements. From Table 1, the average current and voltage were 101.325 mA and 0.216 V respectively and the average resistance was 2.189 Ω. This value was rounded to 2.19 Ω for all subsequent calculations.

Position	Current (mA)	Voltage (V)	Resistance (Ω)
1	78.3	0.25	3.1928
2	117.2	0.193	1.6468
3	107.2	0.207	1.9310
4	97.4	0.222	2.2793
5	100.5	0.216	2.1493
6	108.7	0.204	1.8767
7	113.1	0.200	1.7683
8	88.2	0.235	2.6644
Average	101.325	0.216	2.189

Table 1: Motor VI Characteristics to Find Resistance

Next the inductance of the motor was solved for. The most accurate way of solving for the inductance is by creating an LC circuit and finding the resonant frequency. To do this, a function generator outputting a sine wave was wired in series with an ammeter, the motor, a capacitor and a resistor. The ammeter would measure the current using its RMS measurement feature and the additional resistor was to provide a large load to the function generator:

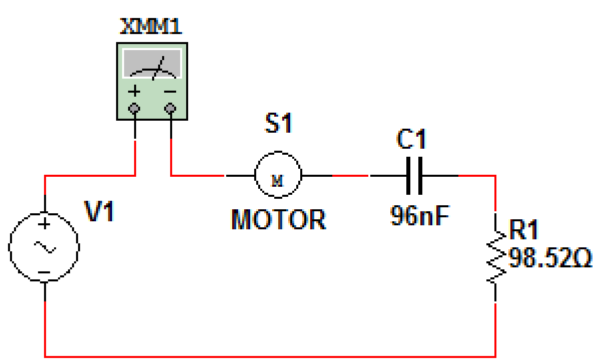

Figure 8: Motor Inductance Test Circuit

The values for the resistor and capacitor were measured to be 98.52 Ω and 96 nF respectively. The resonant frequency of the circuit would simply be the frequency at which the circuit drew the most current. Varying the frequency of the function generator, this frequency was found at 15.8 kHz. Following the equation for resonant frequency:

$$\omega_R = 1 / (L*C)^{1/2}$$

The inductance of the motor was calculated to be 1.057mH.

Following this calculation, the back EMF constant, k, of the motor needed to be found. The back EMF constant holds a linear relationship with the rotational speed (ω) of the motor. The equation during a steady state is:

$$V = Ri + k\omega$$

Where V is the total voltage across the motor, i is the current through the motor and R is the resistance of the motor.

To find the constant k, the voltage and the current for the motor were measured over different speeds using the same circuit as in Figure 8. The speed of the motor was calculated by attaching a small disc to the shaft of the motor and putting a single mark on it. Using a strobe, an LED powered by a square wave from a function generator, the exact rotational speed was calculated based on the frequency of the strobe then the mark appears to not move. From here, the value of k could be found for each speed and averaged. Table 2 shows the results of these measurements and the constant k was averaged to be 0.0212 Vs/rad.

The final measurement of the motor was the mechanical damping inherent in the unloaded motor. At a constant speed the damping is almost exactly equal to the torque generated by the motor. The torque generated is equal to the back EMF constant times the current through the motor:

$$ki = D\omega$$

Where D is the damping factor. From the measurements in Table 2, the damping factor D was also calculated and it was found that it changes with respect to the speed.

Frequency in Hz	Voltage in V	Current in A	ω in rad/s	k in Vs/rad	D (ω)
1.230E+01	1.980	0.179	7.728E+01	2.069E-02	4.791E-05
1.770E+01	2.750	0.182	1.112E+02	2.124E-02	3.476E-05
1.926E+01	2.930	0.184	1.210E+02	2.097E-02	3.189E-05
2.126E+01	3.220	0.185	1.336E+02	2.116E-02	2.930E-05
2.478E+01	3.690	0.184	1.557E+02	2.118E-02	2.503E-05
2.702E+01	4.010	0.183	1.698E+02	2.132E-02	2.299E-05
3.042E+01	4.510	0.185	1.911E+02	2.153E-02	2.084E-05
3.295E+01	4.880	0.189	2.070E+02	2.163E-02	1.974E-05
4.324E+01	6.280	0.193	2.717E+02	2.160E-02	1.535E-05

Table 2: Unloaded Motor Measurements to Find Back EMF and Inertia

The results for D (ω) were plotted over angular velocity in Figure 9 to observe their relationship. The line of best fit was the equation D (ω) = 0.0025 $\omega^{-0.912}$ showing an almost linear relationship over the speeds measured:

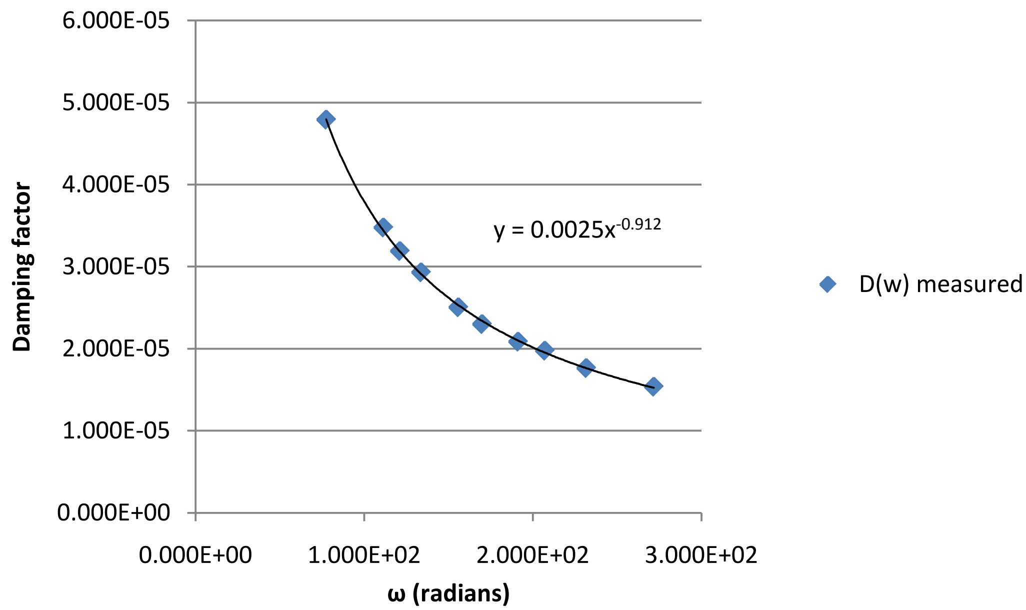

Figure 9: Inertia versus Angular Velocity (Unloaded Motor)

Therefore, from the equation for D (ω), the equation for D(ω) · ω is equal to:

$$D(\omega) \cdot \omega = 0.0025\ \omega^{0.088}$$

From these measurements, a motor simulation could be created. The simulation comprised of two circuits, one representing the electrical system and one representing the mechanical. The resistance and the inductance of the motor were put in series with a voltage source and a current-dependent voltage source that represents the back EMF. The mechanical circuit is composed of another current-dependent voltage source to represent the torque generated by ki, a inductor to represent the very small amount of rotational inertia the motor has and a final current-dependent voltage source to represent D(ω) · ω. One small resistor, of value 1µΩ was added to the circuit to ensure the graphs would converge. These two circuits were put into PSPICE and a transient analysis was done on the circuits. The code for the PSPICE simulation can be found in Appendix A.

With the voltage to the motor going from 0V to 12V at time 0s, the current and the speed, which is represented as a current, are plotted over 0.3s. Beyond this point and the two reach constant values. In Figure 10, the current is plotted on the top and the speed below.

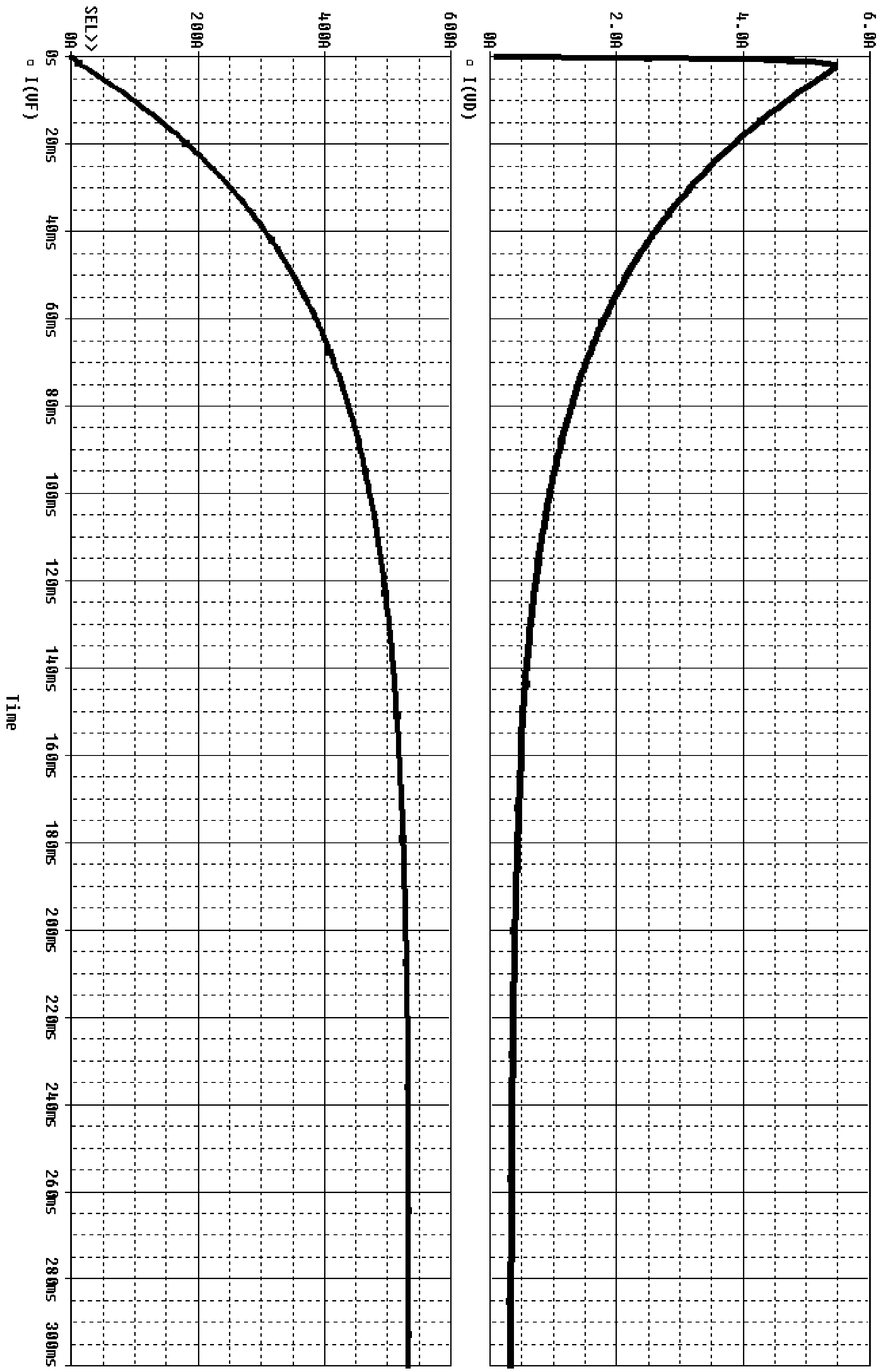

Figure 10: Simulated Motor Start-Up Current and Speed

It should be noted that no additional motors were tested for this project. The two DC motors were donated to the project and met the project requirements. However, with further development other motors should be tested, which could possibly reduce cost and increase efficiency. One possible alternative that was originally considered would be using stepper motors for movement.

3.1.2 Rubber Belt

In the first prototype, a DC motor and pulley system was used. A circular wooden platter with an approximate diameter of 6 inches was mounted on a metal tube. The tube sat on a shaft machined to fit snugly within the inner diameter of the tube to form a rudimentary spindle assembly. The spindle was lubricated so the platter could freely move. A thin rubber belt was wrapped around the platter as well as around a pulley on the DC motor that was mounted next to the platter, less than an inch away.

This system was tested with a 5V source with a 0.5A current limit. The motor was able to rotate the platform, however, with higher voltage levels the platter rotated at a velocity that was far too fast for small, precise movements required by a tracking system. When this setup was tested with the later described circuits, there was a significant amount of jitter due to the fact that the system moved too fast to make precise adjustments. Another problem was that the rubber belt occasionally detached from the platter and motor, mainly due to using a rubber belt with an inadequate size and flexibility.

From this, an alternate method needed to be used for the system. A small rubber wheel was substituted for the pulley on the motor and it was situated so that the wheel rubbed against the platter. This essentially formed a gear coupling with the platter and gave the whole system a slightly less amount of free-play in the rotation. However, this system still spun much too fast even at 5V for the system to adequately track without jitter.

Since none of the attempted setups above worked well at the higher voltages the system meant to run at, an alternative method needed to be found. The main problem that the rubber belts encountered was the mechanical damping was not great enough to counteract the inertia of the platter when the power to the motor was terminated. This led to the next setup using worm gears.

3.1.3 Worm Gears

Worm gears are capable of high speed-reduction ratios as well as ensuring that there is no inertial backlash to the driving source. This is ideal for a solar tracking system as the tracker needed to move both slowly and with minimal influence from inertia. For this project two different worm gear sizes were tested. The worms were the same ones for both setups.

In the first setup a 1 inch worm along with a 1 inch plastic worm gear with a reduction ratio of 50:1, was used. For this setup the entire azimuth axis was rebuilt, this time out of acrylic. Another alteration that was made was the position of the motor. Previously it had been off the platter, but this lead to the necessity of long, flexible wires to the motor that also restricted 360° movement. For this new design, the motor was placed next to the worm gear that was attached to the shaft at the center of the platter. With initial tests this setup seemed to move a lot smoother than the previous setups, but the angular velocity was still too fast and the system could not respond quick enough.

While the possibilities for improving the azimuth axis were considered, a wooden prototype for the altitude axis was built also using the motor and worm gear setup. The weight of the solar sensor array added a significant load to the motor and lead to slower rotational speeds but at the cost of more power being used. During testing, the altitude axis exhibited a more accurate, slower angular velocity than the azimuth axis, but still seemed a bit too fast.

In order to reduce the speed even further, 5 inch brass worm gears with a 180:1 reduction ratio, were substituted in for both axes. The new worm gears were first tested with the azimuth axis and proved to be highly effective. The platter moved at a much slower speed which meant the tracker could stop the motor before it overshot the light source. Since this was an effective solution, the altitude axis was reconstructed using acrylic and the larger worm gear. This setup shoved marked improvements over the previous version as well.

One down side to the larger gears was the significant increase in cost. In future development the use of different motors and driving methods will produce a lower material cost.

3.2 Electrical System

To produce a useful solar tracker the electrical system needs to give accurate control signals to the mechanical system, be reliable, and have low power consumption. Since analog systems deal with continuous voltages, this seemed ideal for providing smooth and accurate control of the mechanical system. Thus, the initial electrical system consisted of solar sensors, a comparator circuit and an H-bridge. To improve this system's performance some modifications were implemented: different solar sensors, different solar sensor arrangements, hysteresis to the comparator, and pulse width modulation (PWM) for more precise motor control. Later in the design process the analog comparator circuit was replaced with a digital microcontroller for improved efficiency. Although the original electrical system was put on breadboards, the final system used two printed circuit boards (PCBs) to ensure reliability.

3.2.1 Power Supply and Motor Control

In the initial design of the tracker, it incorporated a rechargeable battery to power the tracking system. The battery would be recharged by the solar panel mounted on the tracker so the system would be self-sufficient. To choose a battery, the power supply voltage had to be chosen that allowed the tracker to operate in entirety. During the testing phase of this project, 5V was chosen arbitrarily as a starting point to help design the circuits. As the project progressed, batteries were examined for the tracking system and exactly 5V batteries are hard to find in a rechargeable package.

Taking into consideration that the tracker would be operating in remote parts of the world and the battery would have to be replaced eventually, the power supply was changed to a readily available 12V battery. However, in lieu of time and budget restrictions, the battery charging system was not incorporated in the final tracker prototype. 12V was kept as the power supply voltage so in the future; a rechargeable battery can be implemented into the tracking system.

As described previously, the motor chosen was a DC motor. This motor can rotate in both directions by reversing the direction of the current supplied. Because the power supply on the tracking system has only one pole, a circuit was needed to switch the direction of the current to the motor. The most power efficient way to accomplish this is with a circuit known as an H-bridge which a simplified schematic is provided in Figure 11.

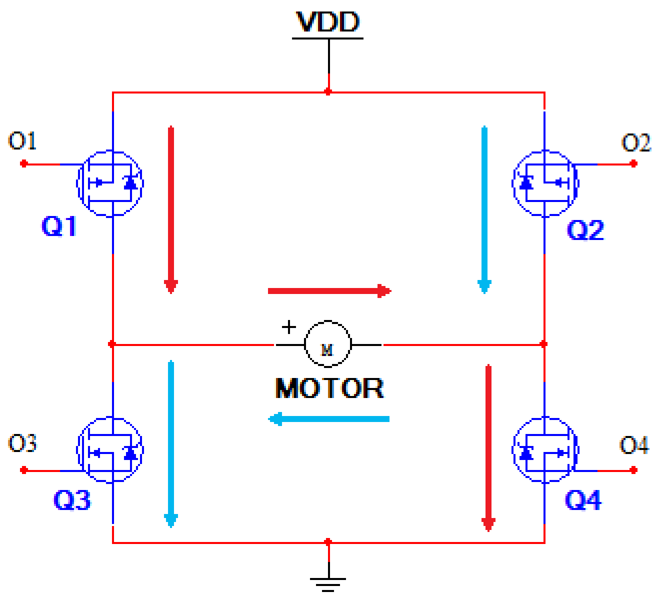

O1	O2	O3	O4	Current Path
Low	High	Low	High	
High	Low	High	Low	

Figure 11: Basic H-bridge Circuit

Here, two pairs of MOSFETs work in conjunction with each other to provide a current through the motor in a certain direction. The upper MOSFETs are P-channel devices and the lower devices are N-channel. Using P-channel devices negates the need to use a voltage doubler to get the gate voltage high enough to turn the device on. When one P-channel MOSFET allows current to pass through and the N-channel MOSFET diagonally across from it also does, the motor spins in one direction. If these are both turned “off” and the other two MOSFETs turned “on”, the motor spins in the opposite direction. The table in Figure 11 above shows what current paths coordinate with which voltage values at the gates of the MOSFETs.

For the H-bridge, the transistors chosen had to be both power efficient fit with the mantra of the project as well as inexpensive and widely available for production reasons.

MOSFETs were chosen for their high power efficiency compared to other transistor technologies like the Bipolar Junction Transistor (BJT) which actively draws current in addition to the current flowing through the device. Within the range of MOSFETs there are also power MOSFETs with a different internal construction that give them high current and/or high voltage capabilities. These power MOSFETs generally have a much lower on-resistance than standard MOSFETs and therefor have a lower power dissipation and higher efficiency. To further improve power efficiency, a complementary pair was chosen. Complementary transistor pairs are two devices, in this case, one N-channel and one P-channel MOSFET, that are made in a way so that they operate as near identical opposites of each other. For this project where the MOSFETs are acting as switches, the pair switches at the same speed. Based on previous experience, this quality is especially important to prevent the shorting of the H-bridge. If the P and N-channel MOSFETs on one side of bridge switch at different speeds, one MOSFET can stay on for too long of a time and when the other MOSFET turns on, the H-bridge can short and burn out one of the transistors. A complementary pair negates this by ensuring that there is always some amount of resistance between the two power rails during switching.

Another major consideration in choosing the MOSFETs was the power consideration. The internal on-resistance of the MOSFET determines how much power is dissipated as heat when current is flowing through the device. For maximum power efficiency, the amount of power dissipated has to be minimal and therefore the resistance has to be minimal. Additionally, this dissipated power can damage the MOSFET if the device is not properly cooled. For cost purposes, both heat sinks and active cooling systems were avoided and MOSFETs were chosen that had a low enough power dissipation such that they did not require additional cooling measures. For this the thermal resistance of the devices has to be taken into account.

The thermal resistance is a measure of how many degrees in temperature the device will rise in relation to the ambient temperature when dissipating a certain amount of power, measured in Watts. Because there will be no heat sinks on the H-bridge, the total thermal resistance will be from the device junction to the air. This measure is often included in device datasheets as $R_{\theta JA}$. The lower this measurement, the more power can be dissipated without additional cooling. To calculate the maximum allowable thermal resistance, the equation is:

$$\Delta T / P = R_{\theta max}$$

Where P is the power dissipated by the device and ΔT is the difference between the ambient temperature and the maximum operating temperature of the device. Knowing that the tracker will be operating near the equator where record high temperatures have been recorded; the ambient temperature in the worst case scenario can take the value of 50°C. Also assuming the MOSFET has an atypically low maximum operating temperature of 125°C, then ΔT under the worst-case conditions is 75°C. The power dissipated by the device can be calculated as the product of the internal resistance and the current squared:

$$P = I^2 R$$

Knowing that the maximum current drawn by the motor during testing was ≈400mA, the equation to calculate the maximum thermal resistance is now:

$$25°C / (0.160 * R_{ON}) = R_{\theta max}$$

Power MOSFETs typically come in a non-insulated TO-220 package which has a typical thermal resistance junction-to-air of ≈65°C/W. Therefore $R_{\theta max}$ > 65°C/W. Plugging this inequality into the above equation and solving for R_{ON}, the minimum on-resistance can be calculated as:

$$R_{ON} < 2.404\ \Omega$$

This calculation is a maximum rating that the power MOSFETs used in the H-bridge can have assuming their maximum operating temperature is 125°C and the thermal resistance junction-to-air is 65°

Taking these specifications into consideration and keeping in mind that any components chosen have to be available across the world to reduce repair costs, the power MOSFETs chosen was the complementary pair of IRF530 N-channel MOSFETs and IRF9530 P-channel MOSFETs. This pair exceeds the required specifications by a wide margin with a maximum current rating of 12A, maximum operating temperature of 175°C and junction-to-air thermal resistance of 62.5°C/W. Most importantly, this is a widely used pair of power MOSFETs ensuring that they are available to most parts of the world and have a very low cost. Additionally, the specifications of the MOSFETs allow larger motors to be used for scaled-up tracking systems without significant electrical changes to the electrical system. Motors drawing ≈2A of power would still not necessitate additional cooling of the H-bridge even at 50°C ambient temperatures.

However, a problem was encountered of sending an input at the ground voltage to the P-channel MOSFETs to reach the lowest on-resistance which gives the best power efficiency. However, for the majority of the tested control systems outlined below, they could not deliver a signal all the way to ground. For this reason, an NPN BJT on the gate of the P-channel MOSFETs was used to allow the signal to reach ground. In the same sense, an N-channel MOSFET needs to reach the power supply voltage to have the lowest on-resistance. For many of the control systems, and in particular, the microcontroller, they could not send a signal all the way to the power rail. For this reason, an NPN BJT was also added to the gates of the N-channel MOSFETs. This also meant that the inputs to the H-bridge were inverted; a high signal turned on the P-channel MOSFETs and a low signal turned the N-channel MOSFETs on. In keeping with the idea of using widely available parts, the common 2N3904 NPN BJT were used in the H-bridge.

Below in Figure 12 is the schematic for the final H-bridge circuit block. The diodes connected across the drain and source terminals of the MOSFETs are for the inductive kickback from the motor. This kickback is a high voltage spike which can easily damage the MOSFETs. The diodes are so that if the voltage gets above a certain value, they effectively short the motor to the rails and the spike is eliminated. The 1N4004 rectifier diode is ideal for this application because of its high surge current capability and wide availability.

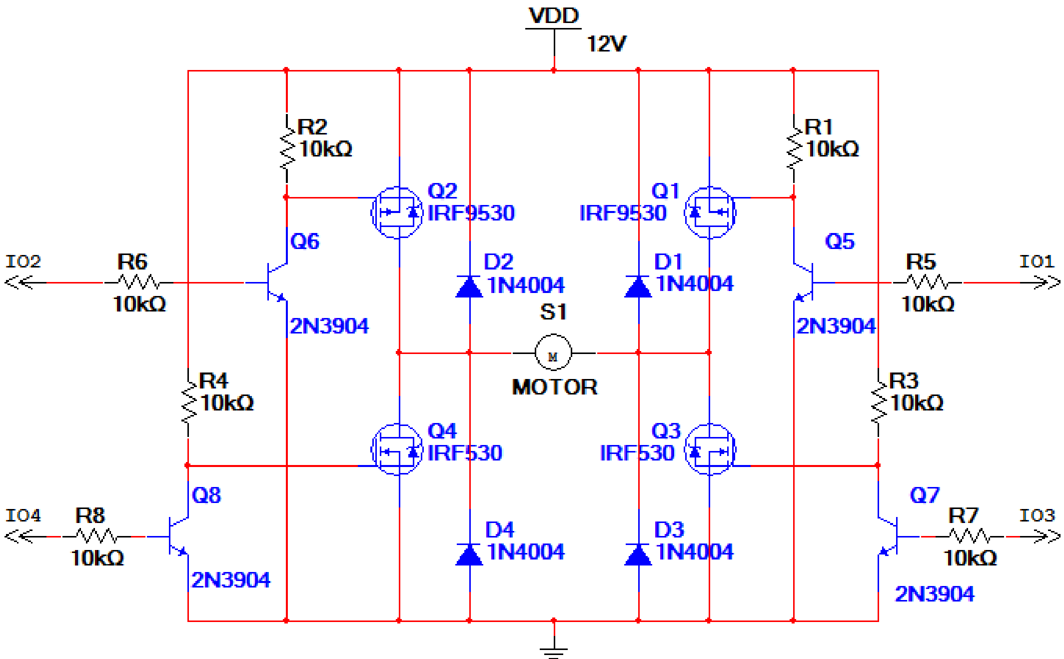

Figure 12: Revised H-bridge Schematic

Because the motor will be moving for a very small percentage of the day, the power used when the H-bridge is "off" or not supplying any power to the motor needs to be minimal. The resistors in the circuit were chosen so that when the H-bridge is off, the current draw is <5mA for efficiency. Testing the circuit with the motor parameters in Multisim shows the total current draw when the H-bridge is "off" is 4.65 mA which is 55.8 mW. Higher value of resistors would lower the current draw but would also increase the switching times of all the MOSFETs which would increase the transient current draw.

During testing, many of the mechanical systems did not move slowly enough given the H-bridge, and in turn, the motor, were being directly supplied by the full power rail voltage. To combat this, reducing the speed of the motor would circumvent the need to make any severe mechanical changes to the system. However, the easiest way to lower the speed of the motor, adding a resistor in series with the motor, lowers the torque of the motor and reduces its ability to effectively turn the system. Using a PWM signal, however, can lower the speed of the motor without having a significant impact on the torque.

When using the analog comparator circuit outlined below in 3.2.3, the PWM signal needed to come from an external source because the comparator could not provide this signal. For this, a 555 Timer was used to create a PWM signal which was then connected to the collectors of Q7 and Q8, through their respective resistors R3 and R4, in the H-bridge circuit above. This system proved to be an effective way to significantly reduce the speed of the motor which allowed the tracker more precise movement.

This PWM generator was later removed as the microcontroller used as the main control unit as described below in 3.2.4, could output a PWM signal generated and controlled internally. This saved power that was being used for the 555 timer and reduced the complexity of the circuit.

Using PWM to control the motor necessitates a power capacitor to handle the surge currents of the motor. When the motor is switching on and off as well as reacting to changes in its mechanical load, the current drawn can change quickly and will drop the voltage the power supply can deliver. The change in the voltage is called the ripple amount and can be alleviated with a capacitor to supply the surge currents. To calculate the ideal value for the capacitor, the equation for the ripple in the voltage supply is:

$$V_{PP} = I_L / (f * C)$$

Where V_{PP} is the peak-to-peak ripple voltage, I_L is the peak current draw, f is the frequency of the oscillations, in this case the PWM frequency, and C is the capacitor's value. The frequency of the PWM used in the final circuit, supplied by the microcontroller, is 500Hz according to the datasheet. The maximum load current is 400mA from the maximum measured current going to the motor during testing. For a desired amount of ripple to be 0.5 volts, less than 5% deviation from the 12V power supply, the optimal capacitor value can be calculated:

$$0.5V = 0.4A / (500Hz * C)$$

$$C = 1600\mu F$$

This capacitor was added between the 12V power rail and ground for both H-bridges used, as seen in Figure 13:

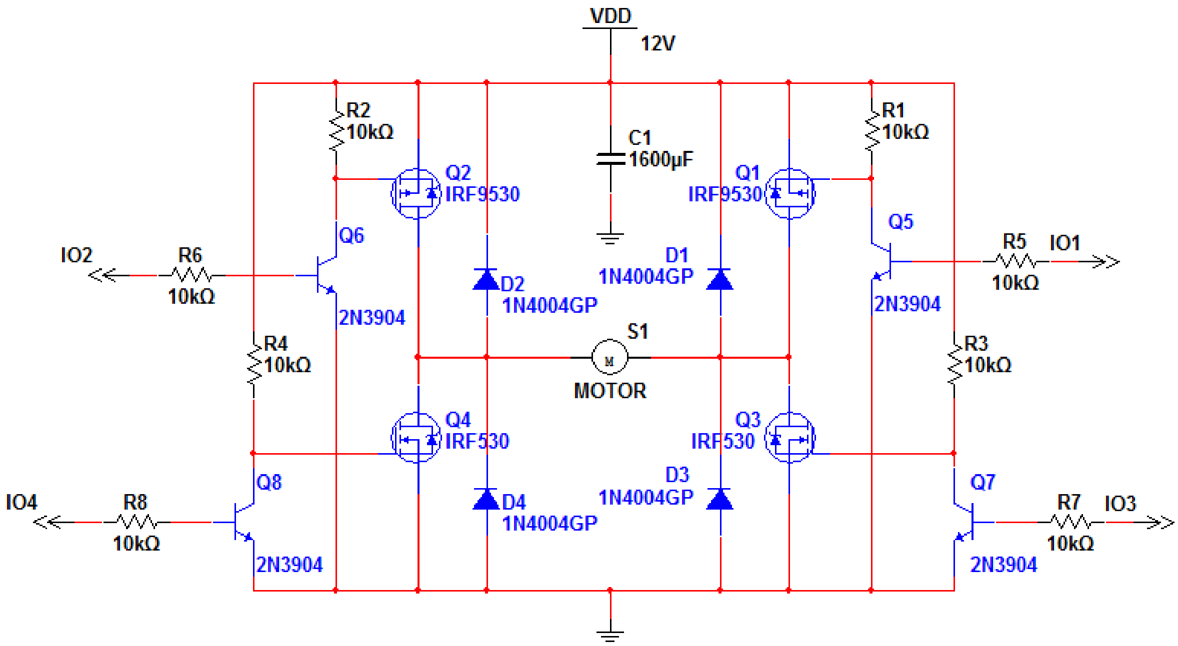

Figure 13: Final H-bridge Schematic

3.2.2 Solar Sensor Array

To provide an accurate and reliable tracking of the sun, a solar sensor array was designed. Based on previous projects, photoresistors and photovoltaic cells were considered as possible sensors. The solar sensors were primarily chosen based on linearity of the output response due to the change in the angle of incidence. The sensor tilt angle was chosen that obtained the highest angular response.

For the initial design, two photoresistors were used, each with a measured dark resistance of 1.36MΩ. These sensors were both mounted perpendicular to the light source, as seen in Figure 14 (left). This setup provided poor accuracy and thus a mount that allowed for adjusting the tilt angle was used, as seen in Figure 14 (right).

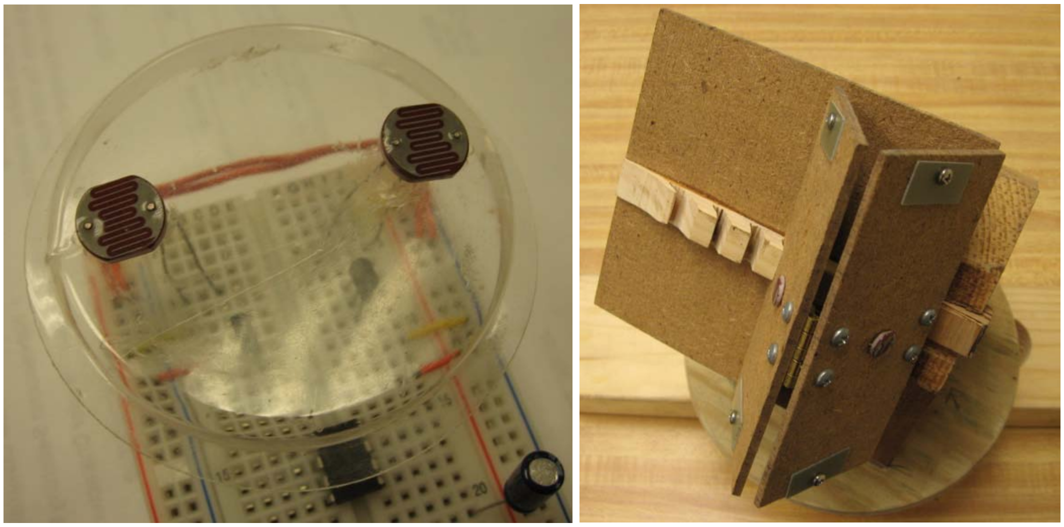

Figure 14: From Left to Right: Perpendicular Photoresistors and Adjustable Tilt Angle Mount

In order to determine a tilt angle that provided the best accuracy and the best response to a change in the angle of incidence a testing setup with a 100 watt light bulb was built. The adjustable mount allowed for tilt angles of 25°, 35°, 45°, 55°, and 65°. The light bulb was positioned approximately a foot from the adjustable tilt angle mount. A separator that was fixed by the mount allowed the light bulb to be rotated around the mount, while maintaining the foot long distance. This setup is seen in Figure 15. The figure represents the angle of incidence as θ and the tilt angle as β.

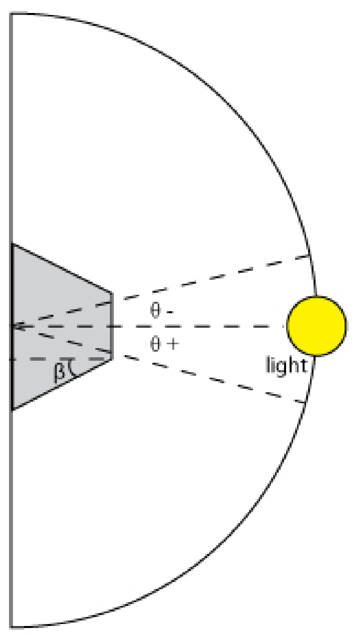

Figure 15: Setup to Test for Ideal Tilt Angle

For testing the photoresistors were each setup in a voltage divider with a 1 V source and a 5kΩ resistor, as seen in Figure 16.

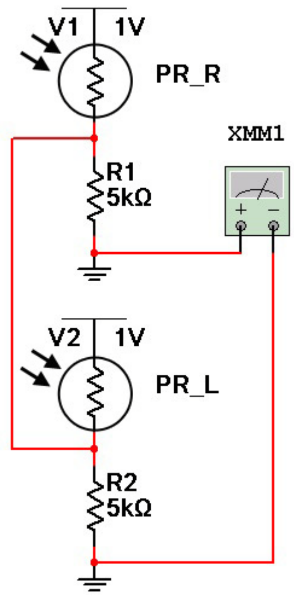

Figure 16: Photoresistor Voltage Divider Circuit

The angle of incidence from the bulb was varied by 5° from -90° to 90° and the voltage difference between the two photoresistor voltage dividers was measured and recorded. This was done for all five tilt angles. These results can be viewed in Appendix A and the resulting graph for the positive angles of incidence is seen in Figure 17. From the graph it can be seen that higher tilt angles are not desirable, since there is only a slight voltage difference at lower angles of incidence.

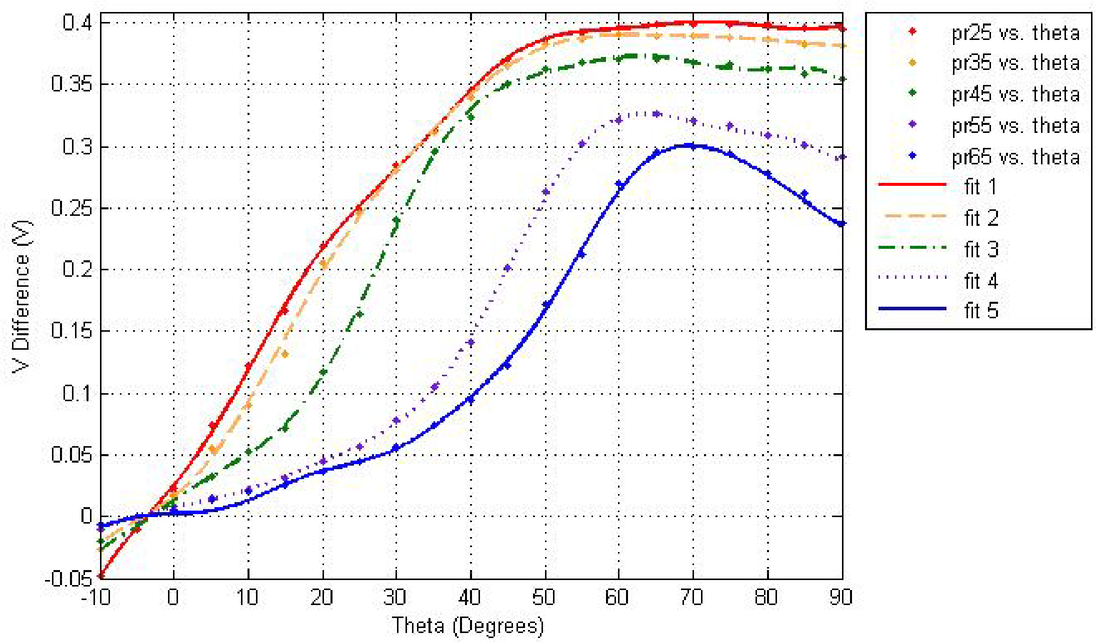

Figure 17: Voltage Difference vs. θ (Photoresistors)

Alongside the photoresistors, two other types of sensors were tested. Two thin film photovoltaic cells and two polycrystalline photovoltaic cells were separately tested. The photovoltaic cells were connected in series with the positive terminals connected, as seen in Figure 18.

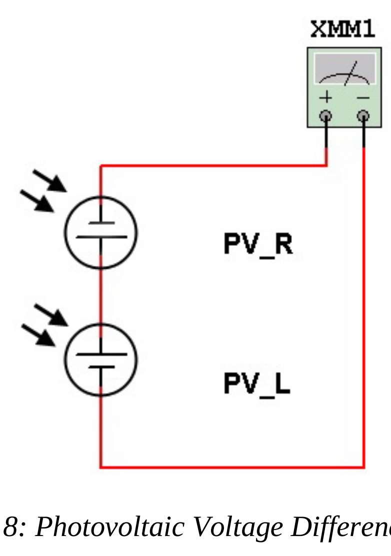

Figure 18: Photovoltaic Voltage Difference Circuit

Besides this the same setup was used as for the photoresistors and the same angles were tested. The gathered data can be viewed in Appendix A and are plotted in Figures 19 and 20.

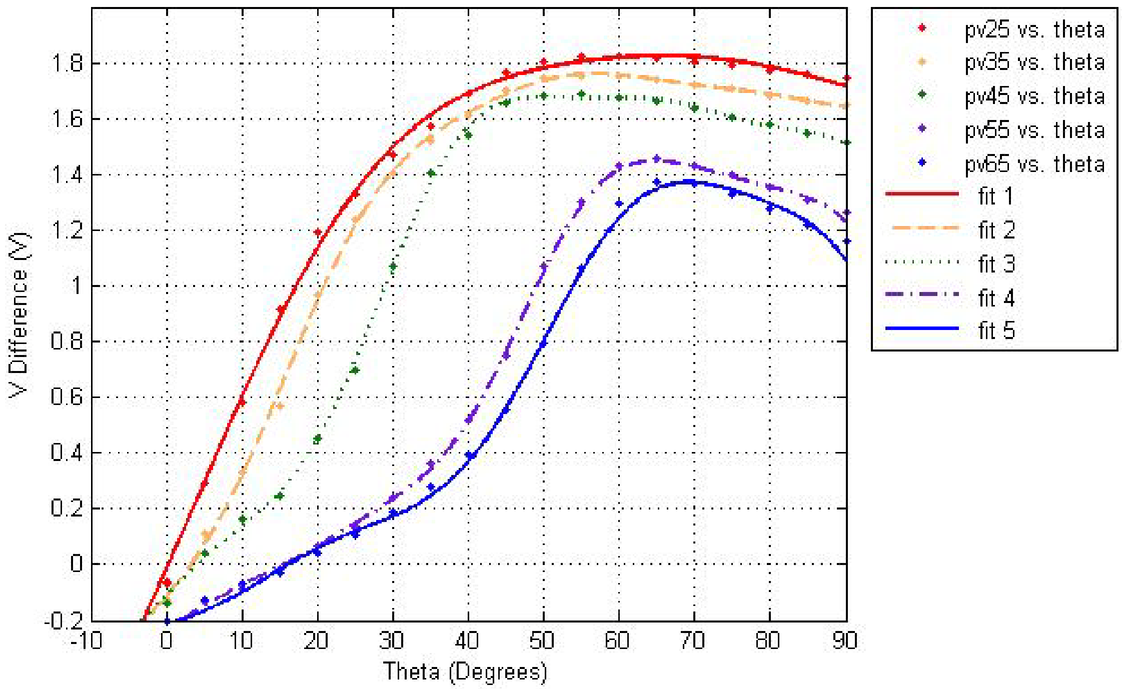

Figure 19: Voltage Difference vs. θ (Thin Film Photovoltaic Cells)

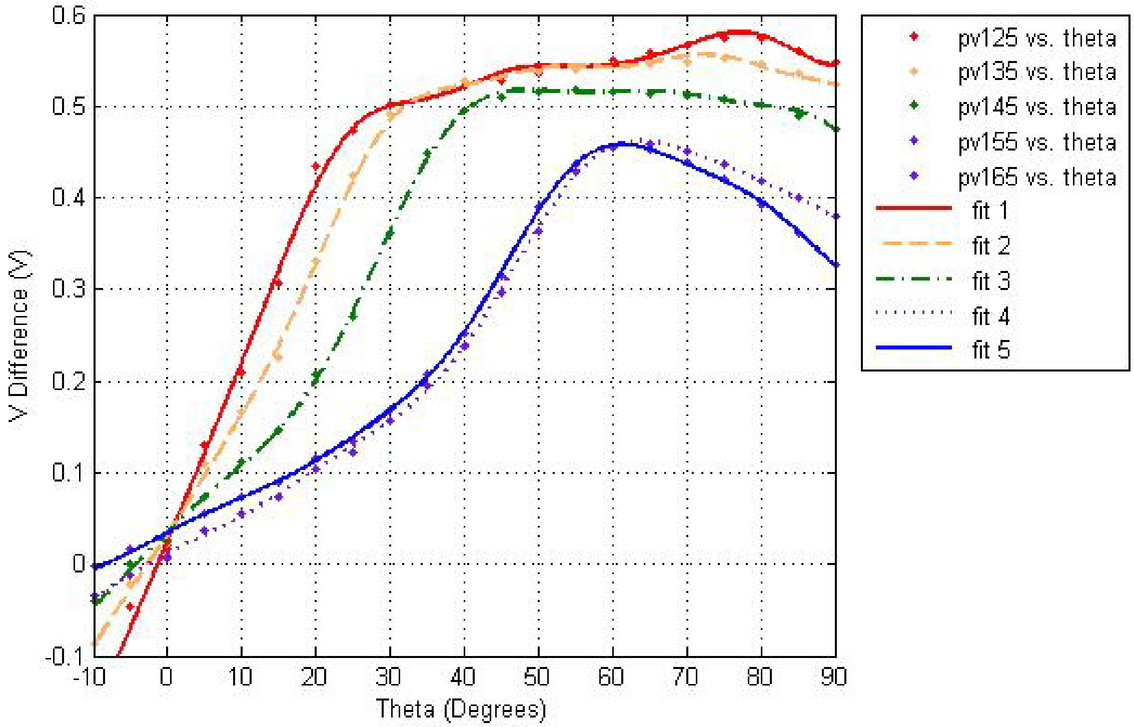

Figure 20: Voltage Difference vs. θ (Polycrystalline Photovoltaic Cells)

The linear portion of these graphs is most favorable, since this portion is when the sensors are reliable and accurate. The slope of the linear sections determines how sensitive the sensors are to the change in the angle of incidence. For all three sensors the tilt angle of 25° seems to provide the most linearity and the steepest slope. Both types of photovoltaic cells provide a more linear response than the photoresistors. To accurately determine the best sensor candidate the derivative of the above graphs were taken during the apparently linear section between -10° to 20°. These graphs can be seen in Figure 21 – 23.

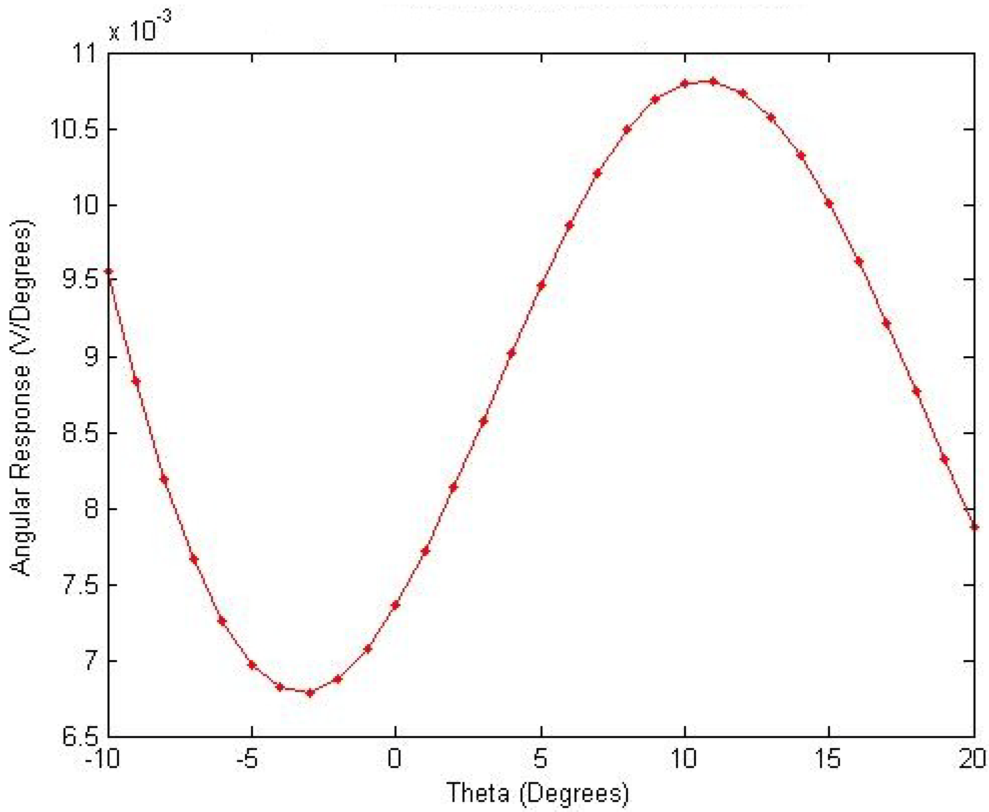

Figure 21: Derivative of Voltage Difference (Photoresistors)

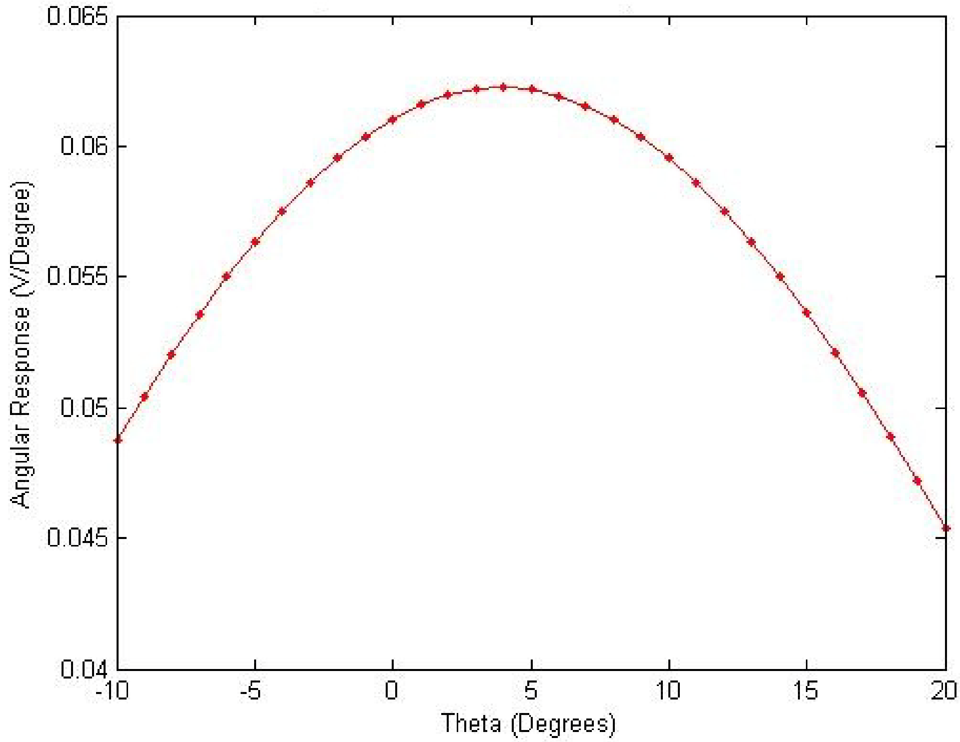

Figure 22: Derivative of Voltage Difference (Thin Film Photovoltaic Cells)

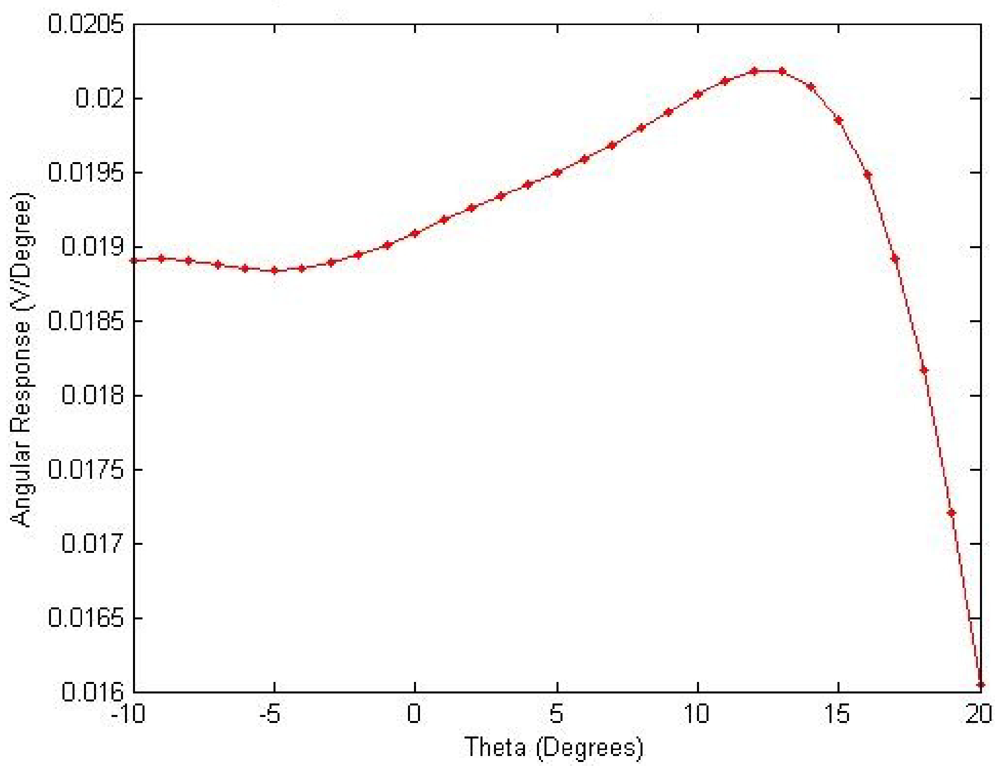

Figure 23: Derivative of Voltage Difference (Polycrystalline Photovoltaic Cells)

It is apparent that the photosensors don't have good linear responses. However, the polycrystalline photovoltaic cells seem to have the flattest response with near constant sections. It is important to note that the thin film photovoltaic cells seem to have the highest angular response at a max of about 0.0625 V/Degree. This is inherently due to the fact that they have a higher short circuit voltage than the other two sensors.

Based on this testing it was determined that to obtain the most accurate and reliable sensor array, two polycrystalline photovoltaic sensors tilted at 25° would be used for use with both the azimuth and altitude axis. The final sensor array was fashioned into an acrylic four sided pyramid, as seen in Figure 24.

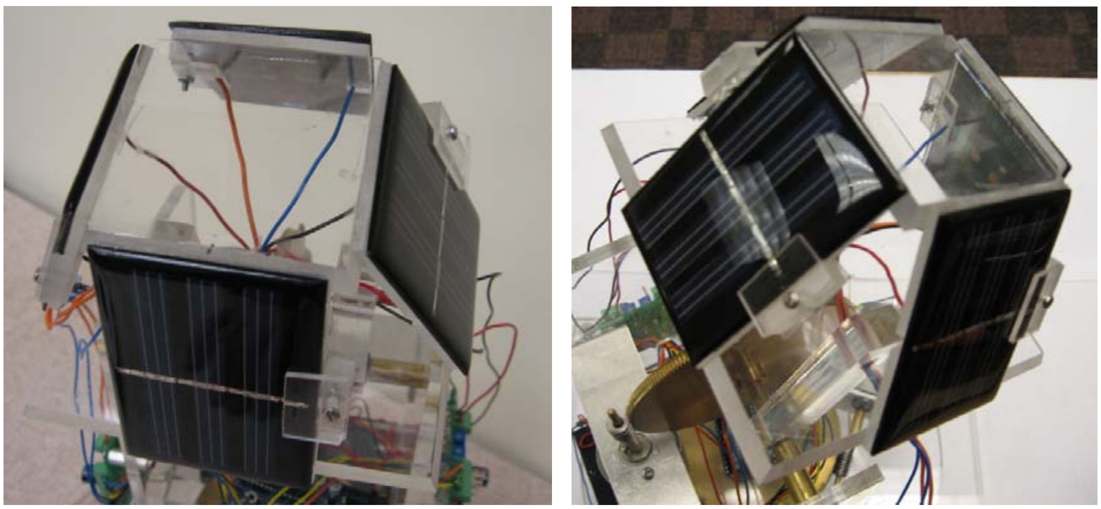

Figure 24: Sensor Pyramid Array

It is possible that other types of photosensors could provide more desirable results. There are also other methods of getting differential illumination results from solar sensors. These methods were considered, but never fully tested. The setup and sensors used in this project may not provide the best results, but they do provide desirable results for the purpose of this project.

3.2.3 Analog Comparator Circuit

To provide an interface from the solar sensors to the H-bridge, a circuit that compares the voltage of two photosensors and outputs a control signal to each of the four MOSFET inputs of the H-bridge had to be designed. This circuit design needed to accurately sense the voltage difference between the photosensors and provide reliable inputs to the H-bridge. The first section of this circuit, that detects the voltage difference, is composed of an analog comparator circuit. The second section, that provides the control inputs to the H-bridge, consists of logic gates.

As mentioned in section 3.2.2, two photoresistors were initially used as photosensors. In obtain a voltage that depended on the resistance change of the photoresistor, a voltage divider was designed. This voltage divider was supplied by 5 V, due to convenience. A 100 kΩ potentiometer was used to complete the voltage divider. This potentiometer is used for calibration, since the photoresistors were not exactly matched and the value was chosen to reduce current through the circuit. At the output a 51 kΩ resistor was used as current protection.

The LM741 is a common operational amplifier with a power dissipation of 500 mW. Two LM741 were connected to the two sensor voltage dividers and configured in the no-feedback, comparator setup. This comparator setup has an overall power dissipation of 1 W.

Since the sun rotates at 2π radians / 24 Hours or 7.272×10^{-5} rad/s which corresponds to a frequency of about 1.16×10^{-5} Hz, the comparator circuit doesn't need to be able to handle fast switching speeds. Since the logic gates can't handle high frequency input signals a low pass filter was designed to allow roughly 10 Hz or lower. Allowing the system to move at higher frequencies wasted power and contributed to jitter in the tracking. A 1 μF capacitor was used and the following calculation was used to calculate the resistor.

$$R = 1/(2\pi \times 10\text{Hz} \times 1\ \mu\text{F}) = 15.9\ \text{k}\Omega$$

Therefore a 15 kΩ resistor was used in the low pass filter.

The output from the comparator circuit are not necessarily discrete, thus an N-channel MOSFET was used to ensure this. The ZNN2110A N-channel MOSFET was chosen since it is readily available and has a power dissipation of 700 mW. Since two were used for each comparator there is an overall power dissipation of 1.4 W. Finally, two red LEDs were used to indicate the photosensor with the highest light intensity. When the light intensity was greater on one photoresistor, the respective LED would turn on, while the other LED turned off. When the light radiation was equal on both photoresistors, both LEDs turned on. A red LED was used since it requires approximately 1.6 V, which is the lowest voltage required compared to other colored LEDs. The red LED requires about

20mA of current and thus the closest resistor of 200Ω to the following calculations was chosen.

$$R = (5\text{ V} - 1.6\text{ V})/20\text{mA} = 170\Omega$$

The schematic for this combined circuit is seen in Figure 25.

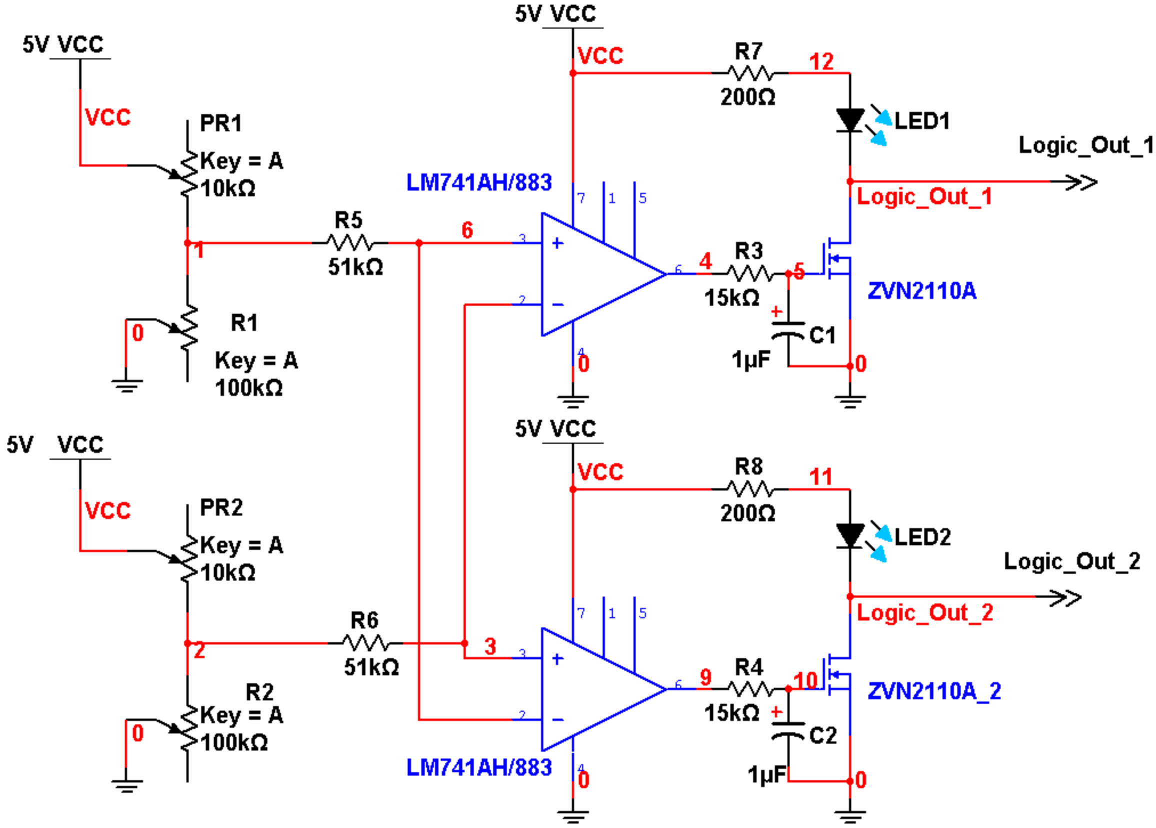

Figure 25: Original Analog Comparator Schematic

A few modifications were made to this comparator circuit. The two LM741 op-amps were replaced with a single LM358 dual op-amp. This was done to reduce the space used and the LM348 has a lower power dissipation of 830 mW. Another alteration was that the inverting inputs were set to an adjustable voltage source. The reason for this was that to put the system at rest, the voltages from both photoresistors had to be exactly identical. Without any space to keep the system at rest, the comparator never reached a steady state during testing with a stationary light source. A third change was the use of photovoltaic cells instead of the photoresistor voltage divider setup, which is further discussed in section 3.2.2. Finally, the power supply was changed to a 12 V source, as discussed in section 3.2.1. This modified circuit can be seen in Figure 26.

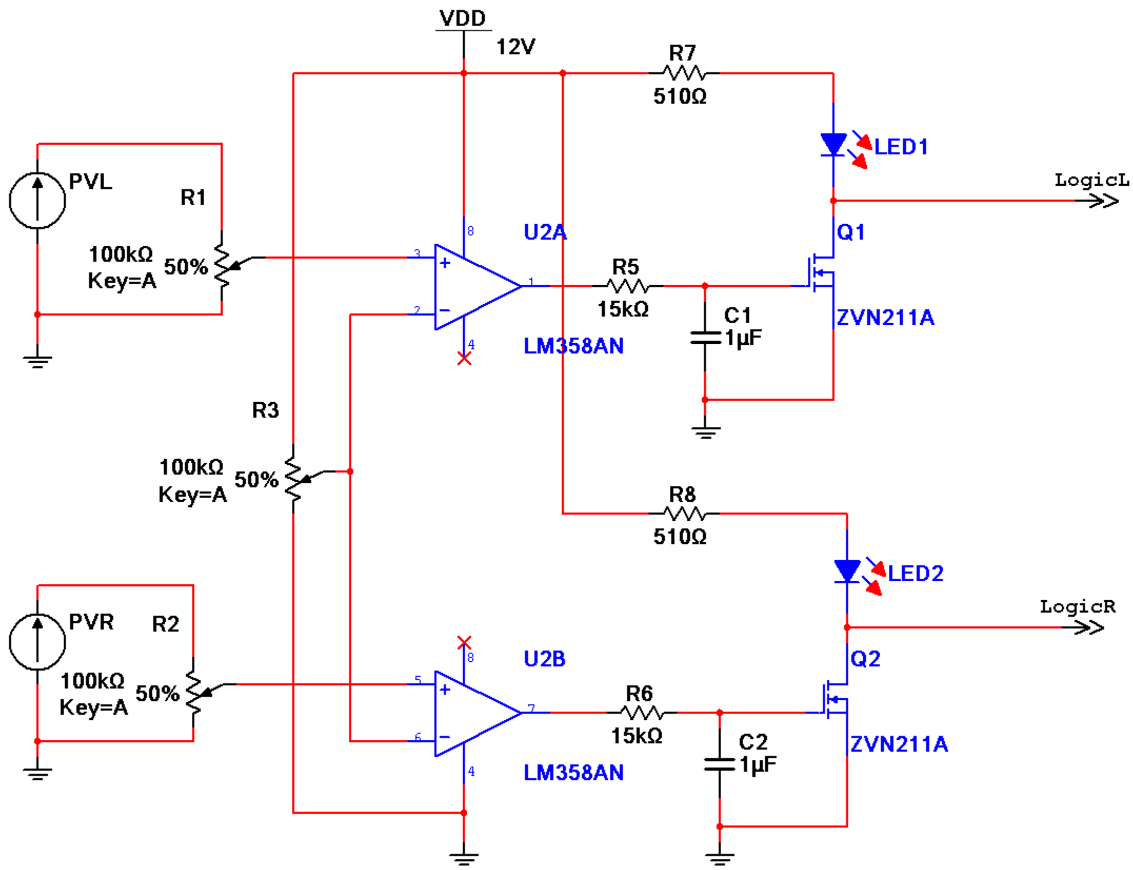

Figure 26: Modified Analog Comparator Schematic

As mentioned earlier the H-bridge requires accurate control inputs to each of the four MOSFETs. However, the above constructed comparator only provides two inputs, thus a set of logic gates were used to obtain the four inputs. When the comparator outputs two high signals, which corresponds to the tracker being pointed at the light source, outputs to the P-channel MOSFETs on the bridge need to go low and the outputs to the N-channel MOSFETs need to go high. If one sensor shows a higher light intensity, the corresponding output goes high. The logic circuit needs to send a signal to the H-bridge to turn on the P-channel and N-channel MOSFETs that correspond to rotation the system in the direction of the light. The reverse goes for the opposite sensor. Finally, when both sensors output a low value, which is impossible, but still needed to be planned for, the H-bridge needed to be shut off in the same fashion as when the sensors outputs are both high. The truth table for the logic needed in is Table 3. Outputs 1 and 2 correspond to the P-channel input and Outputs 3 and 4 go to the N-channel inputs. Output 1 and 3 go to the same side of the H-bridge and 2 and 4 go to the other side.

Sensor L	Sensor R	Output 1	Output 2	Output 3	Output4
0	0	0	0	1	1
0	1	1	0	0	1
1	0	0	1	1	0
1	1	0	0	1	1

Table 3: Comparator Logic Table

Working backward from the truth table, the circuit in Figure 27 was created. It used a combination of inverters, OR and AND gates. At first, the widely available 7400 series of TTL logic chips were used for this circuit. However, it restricted the power supply to 5V which was unacceptable for powering the motor. These gates were swapped with the 4000 series of CMOS logic gates which can operate up to 15V, above the power supply voltage of 12V. The 4000 series logic gates used have a typical power dissipation of 700 mW.

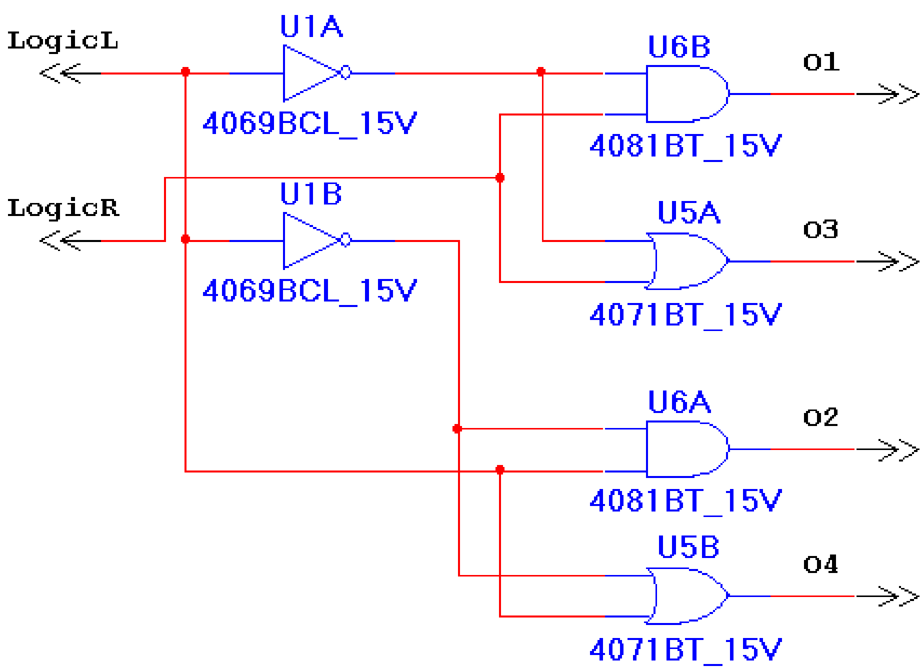

Figure 27: Logic Schematic

3.2.4 Digital System

Because of the drawbacks present in the analog control system, a microcontroller-based, digital control system was also tested. The microcontroller allowed a minimal control circuit complexity, reduced power consumption and allowed for additional features to be introduced to the tracker.

The microcontroller selected had to have at least four analog-to-digital converter (ADC) inputs to take the four signals from the four sensors. It also had to have a minimum of eight digital outputs, four for both of the motor H-bridges. Finally, the microcontroller used had to have a very low power consumption when active to keep the efficiency as high as possible. The most widely available microcontrollers that satisfied these requirements were either AVR or PIC microcontrollers.

For our prototype, a development board for an AVR microcontroller called the Arduino Duemilanove was chosen. The specifications for this development board can be found in Appendix D. The version used has an ATmega 328P microcontroller which has six ADC inputs and 14 digital output pins, six of which can support a PWM output. The board also has an on-board power regulator which can take the 12V power supply directly to supply the 5V the microcontroller needs. The ADC is 10 bits and effective over a 5V range which has a resolution of $V_{Res} \approx 4.88\text{mV}$. This means that the sensors can have a maximum of half this value, or 2.44mV, between them before the microcontroller can detect the change. Knowing that the panels used have a maximum open circuit voltage of 1.44V and assuming a linear relationship between light intensity and voltage produced, the resolution in angle the microcontroller can produce is:

$$\theta_{Res} = \cos^{-1}(1.44 - \tfrac{1}{2} V_{Res} / 1.44) = 3.336°$$

Given the maximum error of 180°, this gives the system an error of 1.853%.

The PWM outputs of the microcontroller in particular allowed the removal of the external PWM generator used in the analog system for a more power efficient and centralized controller. Another major reason this particular board was chosen was the on-board programmer which allowed rapid prototyping during testing of various features for the system. In the future, this development board can be replaced with just a microcontroller with similar inputs and outputs but lower power consumption and without the extraneous circuitry provided on the board.

The microcontroller's function is to compare the voltage levels of the two sensors for one axis of rotation and send the appropriate signal to the H-bridge to move the motor in a certain direction. To reduce the amount of jitter the system has, the microcontroller takes the two voltage values of the sensors and finds the difference between the two. The difference is compared to some reference value. If it is greater than the positive reference value, the microcontroller sends a signal to the H-bridge to move the tracker in one direction. If the difference is less than the negative reference, the microcontroller sends a signal to move the tracker in the opposite direction. Setting the reference to zero will reduce the error to the minimum but it will also introduce significant jitter when a shadow passes over the sensors. Setting the reference to a value greater than zero allows some hysteresis into the tracker but also increases the error. Setting the reference, for example, to 5 means there is a maximum allowable difference between the two sensors of 5 x 4.88mV = 24.4mV. Solving for the difference in angle between the tracker and the sun, this voltage difference corresponds with an angular difference of 0.9945° which is a 0.553% allowable error.

Additionally, the microcontroller examines the voltage outputs of the sensors in relation to night-time conditions. If the values correspond to those during nighttime, the tracker will shut everything off except for the microcontroller to decrease power consumption. This also avoids the problem of the tracker focusing on a nearby nighttime light source such as a streetlamp or building.

The code used for programming the microcontroller is included in Appendix C.

3.3 Final System

An overall system simulation and a final prototype for the tracker were created after deciding what and how to implement each main component of the tracker. The mechanical components consisted of the DC motors, the worm gears and the solar panel sensor array each described above. Electrically, the tracker used the Arduino microcontroller, the H-bridge circuit and non-rechargeable batteries to supply the power.

3.3.1 Total System Simulation

To understand how the tracking system would operate before it was constructed; an ideal simulation was created for one axis of rotation. Only one axis was simulated because under ideal conditions, both axes would operate identically. MATLAB was chosen as the medium for the simulation because it could more accurately simulate the processes of the microcontroller than PSPICE or Multisim.

The first part of the simulation was to collect the specifications of the system. The major portion of the simulation would rely on an accurate representation of how the sensors act during the day. The final panels used had an approximate maximum open circuit voltage of 1.44V as verified through testing. The angle between the backs of the panels is 25° which means that the angle between the normal to the faces of the panels, denoted as gamma (γ), is 155°. If the angle of the sun to some reference point denoted as alpha (α), the voltage across one solar panel can be ideally represented in an equation:

$$V_{PV1} = 0.72 \cos(\alpha + \gamma/2) + 0.72V$$

$$V_{PV1} = 0.72 \cos(\alpha + 77.5°) + 0.72V$$

Inversely, the voltage across the opposing panel can be ideally represented as:

$$V_{PV2} = 0.72 \cos(\alpha - 77.5°) + 0.72V$$

Because cosine is an even function, the voltage difference between the two panels will be zero at $\alpha = 0°$. To incorporate the angular position of the tracker (p) according to the same reference point as the sun, the equations were modified to be:

$$V_{PV1} = 0.72 \cos((\alpha - p) + 77.5°) + 0.72V$$

$$V_{PV2} = 0.72 \cos((\alpha - p) - 77.5°) + 0.72V$$

Now given an angle of the sun and the tracker, the voltage across the panels can be calculated.

Second, the speed of the motor had to be calculated. Putting the motor under load and changing the PWM amounts, the slowest effective speed as at approximately 17% duty cycle. Any slower and the motor could not move the tracker. The measured speed at 100% duty cycle was 5098.2 rpm or 530.74 rad/s. Given the duty cycle and the gear reduction ratio of 180:1, the speed of the tracker is approximately 0.5203 rad/s.

For the simulation, five vectors where created. The first vector is the time vector to show the transient nature of the system. The second is the vector that denotes the angular position of the sun over the duration of the time vector. The rate at which the sun changes its position can be roughly calculated as 360° in a day or 7.272×10^{-8} rad/ms. The position vector is initially set at the reference point and is modified as the simulation progresses. The last two vectors are for the voltages of the panels over time. Each one is calculated from the present value of the sun and the position of the tracker.

The simulation runs the changing sun position through the solar panel equations to get the voltages on the panels at the current position. Simulating the microcontroller, the difference between the two voltages is compared to some reference value that can be changed. If the difference is greater than the reference or less than the negative reference, the simulation increments the position vector at the rate of the tracker speed, 0.5203 rad/s in the direction correspond to which sensor is getting more radiation. If the difference is in between the positive and negative values of the reference, the position is maintained.

After then simulation has run for the specified amount of time, one last vector is created as an error vector. The error is the difference between the sun and the tracker. This vector was converted into degrees for readability.

Using the reference of 5 * 4.88mV = 24.4mV, gamma in radians which is 2.7053 rad and the speed of 0.5203 rad/s, the simulation plots the voltages on the panels, the position of the sun and the tracker next to each other as well as the error of the tracker all over 500 seconds:

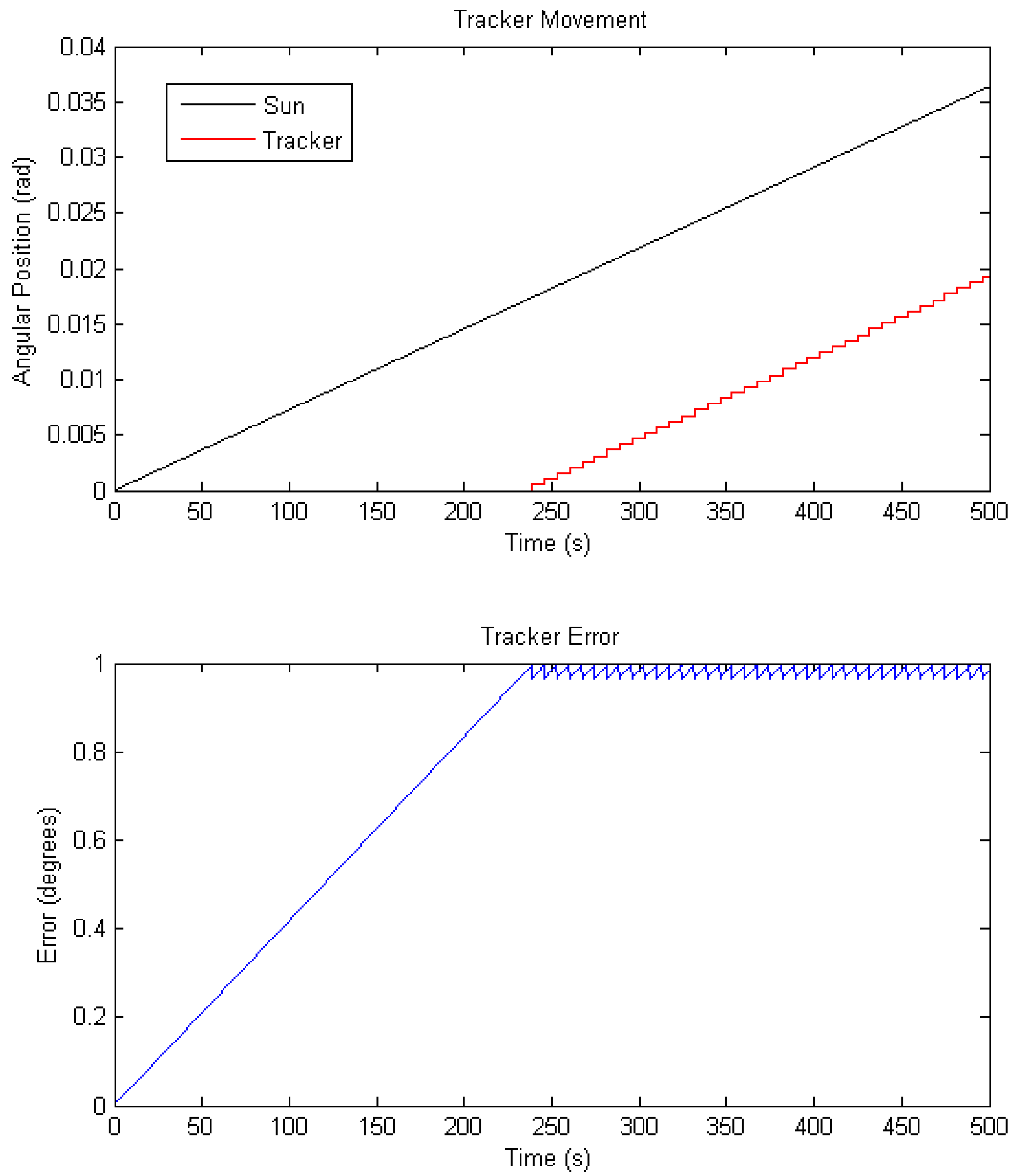

Figure 28: Simulation Results over 500 seconds

The simulation shows that according to an ideal situation, one axis of the tracker works as expected. It follows the sun and maintains a position never more than approximately 1° from the sun. However, the movement of the tracker is stepped in small increments. Zooming in to an interval of 15 seconds, the simulation shows this:

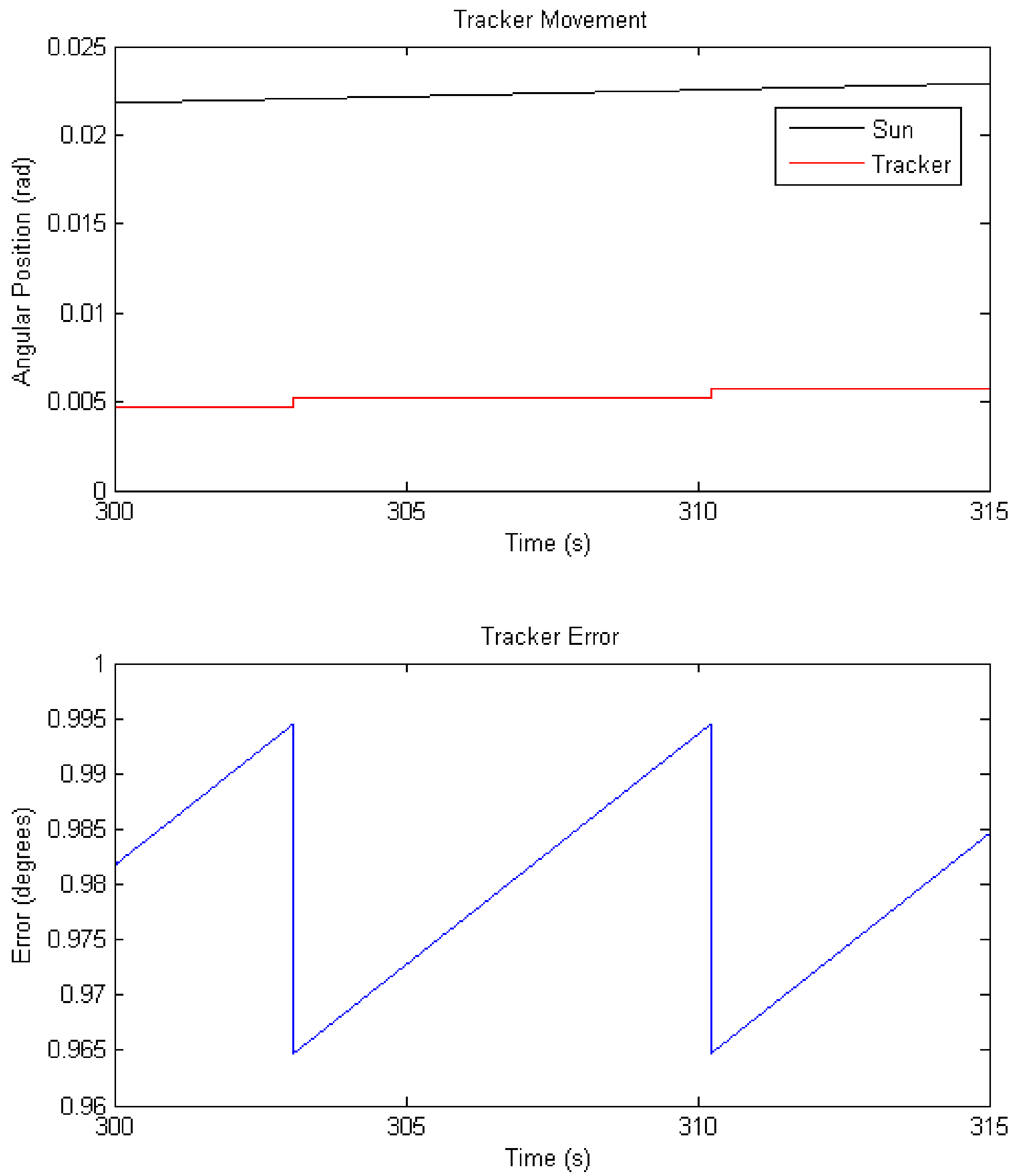

Figure 29: Simulation Results over 15 Seconds

These zoomed in graphs show the tracker jumps in position approximately every 7 seconds. This is a result of the tracker forming a “safe zone” that is 0.9945° off of the sun’s position. When the tracker is within this safe zone, the system is at equilibrium and the tracker does not move. When the sun moves outside of the safe zone, the tracker sees the error and responds by turning the motor on in that direction. The motor spins the tracker back into the safe zone and is moving faster than the tracker can respond so it moves it to approximately 0.965° from the sun, well within the safe zone. The tracker then is at equilibrium until the sun moves too far again and the cycle repeats.

To examine the inner workings of the tracker, it is best to also look at how the panel voltages are reacting over time. Modifying the simulation code to output the solar panel voltages as well as the difference between the two over an interval of 15 seconds, the result is this:

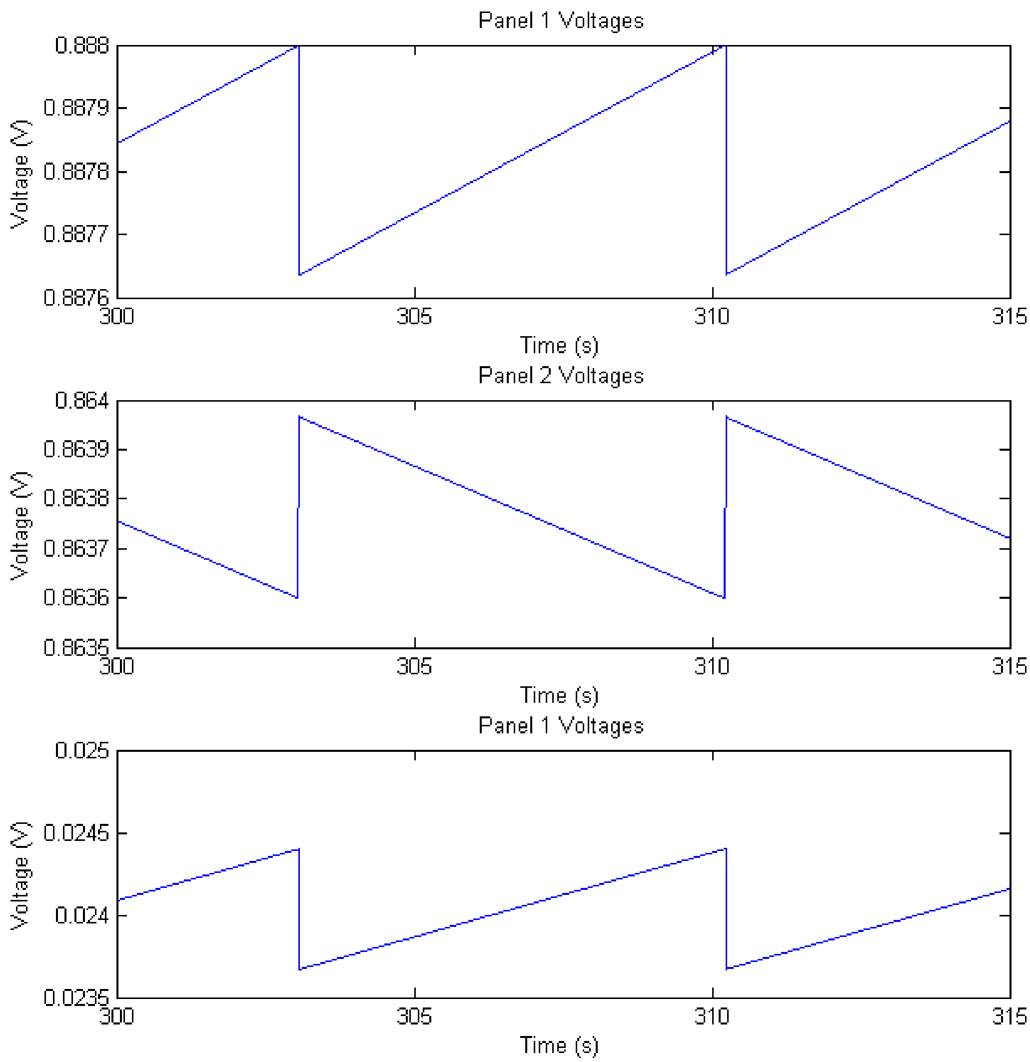

Figure 30: Simulation Panel Voltages over 15 seconds

Panel 1 is the sensor that is closest to the sun during this simulation. If the direction of the sun's movement is reversed, Panel 2 would be the closer. Therefore the simulation is correct in showing that as the sun moves, the voltage on Panel 1 is increasing and the voltage on Panel 2 is decreasing. The difference between these two slowly increases until it reaches 24.4mV at which point the tracker begins to move. The stepped results are still an effect of the motor speed described above.

The simulation shows excellent results that clearly correlate almost exactly to the theoretical calculations done before construction. The MATLAB code for this simulation is included in Appendix D. After verifying the simulated performance, the next step was to construct a working prototype to measure the actual results and compare them with the theoretical.

3.3.2 Construction

The final system design consisted of a mechanical assembly made of clear acrylic to demonstrate the inner workings of the system, aluminum, steel and brass parts for the axle, spindle and motor mount assemblies and the electrical control system which was composed of the microcontroller development board and two custom-made printed circuit boards (PCBs) for the H-bridge and other circuitry. Because a rechargeable battery was not implemented, power to the tracker is supplied by 8, 1.5V alkaline batteries to get the necessary 12V and controlled with a single-pole, single-throw (SPST) power switch.

The PCB was designed to incorporate the circuitry in the smallest footprint possible. The circuits it holds are the H-bridge for the motor, the potentiometers for balancing the signals from the solar panels and two indicator LEDs used for troubleshooting the system. Because the requirements for both axes of the tracker are identical, the PCB was designed for one axis and two were made. This allowed a more compact board size, as well as ensuring that one whole new board need not be made in the event of failure. The PCB layout is seen in Figure 31.

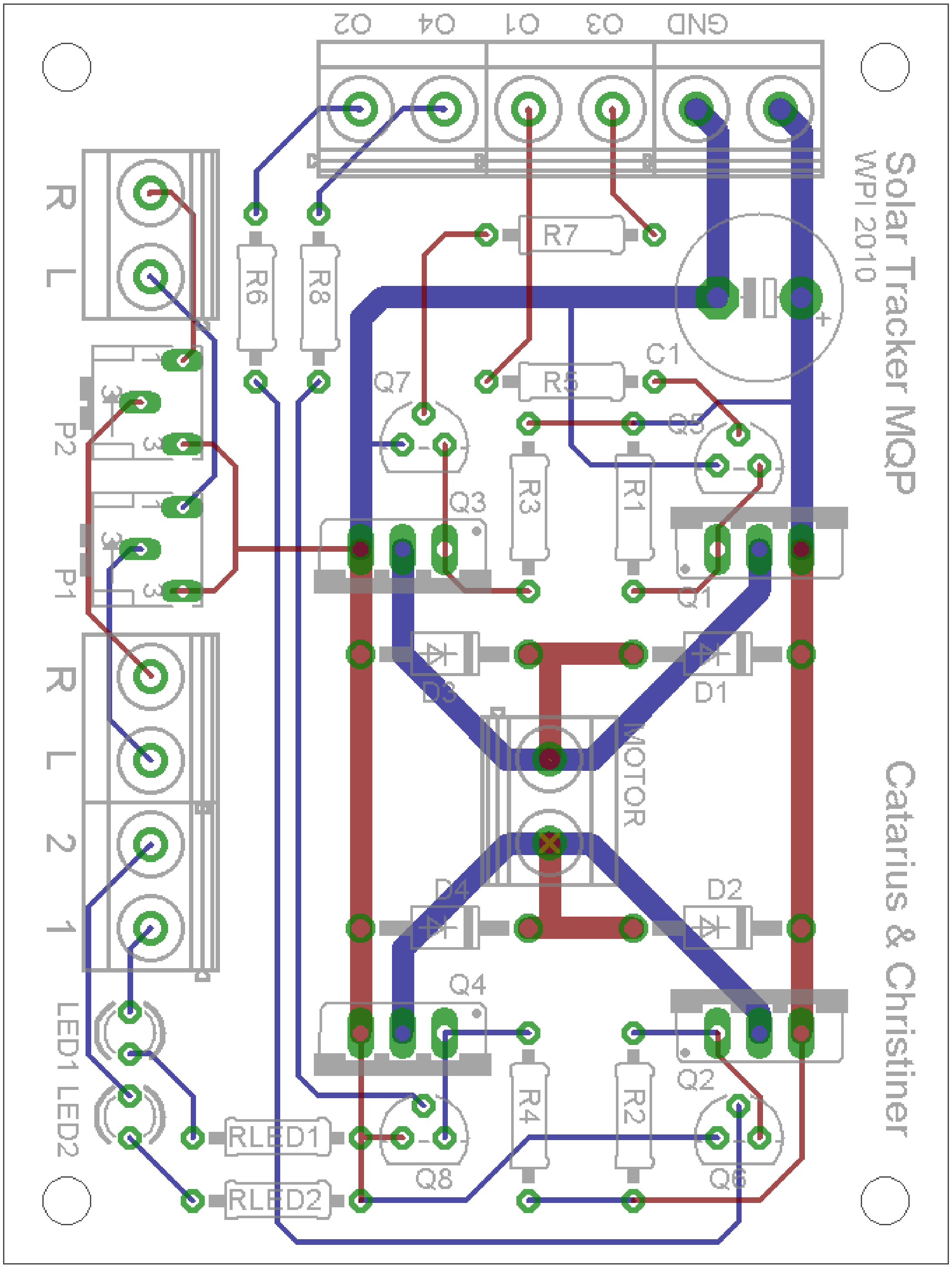

Figure 31: PCB Layout

4 System Analysis and Testing Results

Once the azimuth-altitude dual axis solar tracker was built, the angular error and the power consumption were tested for. The cost of the prototype was analyzed as well. Finally, all the observed drawbacks were noted.

4.1 Functionality Testing Results

After the prototype was built, it was put through several tests of functionality to ensure that it met the original design requirements. The tracker's angular error and power consumption were measured to calculate the tracker's power generation in comparison to other solar panel systems.

4.1.1 Angular Error

The first test of the prototype was to measure the angular difference between a light source and the tracker center, referred to as the angular error. To do this, the altitude axis of the tracker was disabled by removing power to that H-bridge. The altitude axis was also oriented at 90° so that the azimuth sensors were perpendicular with the light source. Then from this, the exact center of the tracker was found and marked by measuring to the exact center of the sensor array and translating that center to the bottom platter using a pendulum.

The test setup comprised of a 100W halogen lamp at the same height as the sensors and kept at 45" away from the tracker using a wooden beam. The beam was notched at one end so it could rotate around the same axis as the tracker. A large protractor was needed to measure the degree difference but there was not one available. So a piece of flat plywood was roughly cut and a protractor was made onto it using a compass a ruler, and a smaller protractor to mark out the angles.

For this test the tracker center was oriented at a starting point and shut off. The light was set to the 0° mark on the protractor so that the error before turning the tracker on was its starting position in degrees. Then the tracker was turned on and its movement to find the light was closely observed. Notable features in the movement consisted of whether or not the tracker “overshot” the light or moved past the 0°, whether the tracker jittered when it got close to the light and if it even reached a stationary point. If the tracker did reach a stationary point, the angle of difference was recorded and the test repeated for the same starting angle in the opposite direction.

The first test was done with a starting point of 45°, the microprocessor reference set at 5 meaning an allowable difference of ≈24.4mV between the panels and the motor PWM amount set at 210 which is a speed reduction of 17.65%. When the tracker was set directly in line with the light, the left sensor input to the microcontroller measured at 0.852 V and the right sensor measured at 0.862 V. Starting counterclockwise, arbitrarily called the negative direction, from the light at 45°, the tracker hit a steady state with an angular error of 2.5° short of the light. Starting clockwise, the positive direction, from the light, the tracker hit a steady state with no discernable angular error to the light.

Increasing the starting point to 75° in both directions, the angular error changed to 3° falling short of the light coming from +75°. Coming from -75°, the tracker actually overshot the light by 1°. This error is obviously due to the mismatch between the two solar panel voltages going to the microcontroller.

Adjusting the voltages going to the microcontroller by using the potentiometers on the circuit boards the left sensor had a voltage of 0.843 V and the right sensor had a voltage of 0.848 V, effectively halving the voltage difference between the two sensors. Again measuring the angular error with the tracker starting at ±75° to the light, the error was 0.5° short of the light coming from -75°. Coming from +75°, the error was 1.5° short of the light.

It should be noted that even with the panels not closely matched, the total angular error calculated by adding the error in both directions was right around 2° which closely correlates with the simulation results of 1° of error in both directions.

To gauge how the tracker would act when the sensors were miscalibrated by a large degree, the potentiometers were adjusted so the left sensor was outputting 0.622 V and the right sensor was outputting 0.735 V. Starting from +75°, the tracker rotated to the right and never reached a steady state. This would be especially hazardous to the altitude axis where the sensor array does not have the clearance to rotate the full 360°.

Narrowing the difference between the sensors so that the left sensor output a voltage of 0.744 V and the right sensor output 0.771V, the same test were performed. Coming from +75°, the tracker stopped 9° short of the light source. Coming from -75°, the tracker stopped at 5.5° past the light source. This shows that miscalibration not only increases the angular error in both directions of rotation but also increases the total angular error of the tracker keeping it only within 4.5° of the light source.

4.1.2 Power Consumption

To ensure that the tracking system actually produced more power than it used, measurements were taken for the power consumption of each individual component of the system. A single 0.49Ω (measured value) resistor was used as a power shunt to measure the current going from the battery to the tracker system as shown in the circuit in Figure 32:

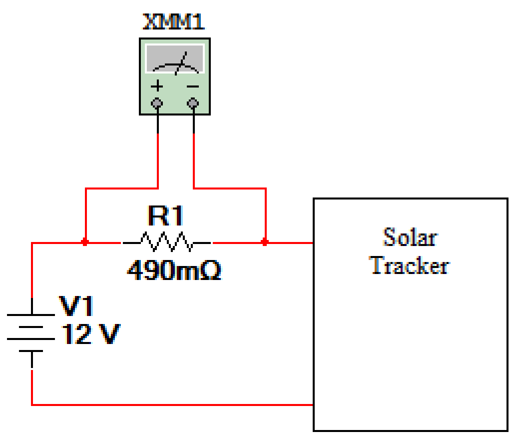

Figure 32: Power Consumption Test Circuit

The voltage measured by the voltmeter, V_{R1}, divided by the resistance gives the current to the tracker. Multiplying the current by the supply voltage, 12 V, the power consumption can be calculated.

Several measurements were taken to find the individual current draws to each section of the system. The first measurements were to the total system, with the shunt between the battery and the rest of the system. The currents were measured when the system was stationary, one axis was moving, the other axis was moving and both axes moving at the same time. To get just one axis to move, the sensor inputs to the microcontroller were incorrectly biased so that the system saw a difference and tried to correct it. For measuring the voltages when the system was moving, the voltages were taken at the highest observed value. The results can be seen in Table 4:

	V_{R1} (mV)	Current (mA)	Power (W)
Stationary	19.4	39.59	0.48
Altitude Axis Moving	98.0	200.0	2.40
Azimuth Axis Moving	147.0	300.0	3.60
Both Axes Moving	196.0	400.0	4.80

Table 4: Total System Power Consumption

From these results, the following can be deduced. The microcontroller, all four indicator LEDs and the quiescent current to the H-bridges consumes 0.48 W when the system is stationary. The altitude axis consumes 2.40 - 0.48 = 1.92W when moving sensors through the maximum load point, or when the sensors are parallel to the ground. The azimuth axis consumes 3.60 - 0.48 = 3.12W at its maximum load point as determined by the friction in the mechanical part. The total power consumption at the maximum load point is equal to 0.48+1.92+3.12 = 5.52W. The difference between this amount and the measured amount is due to the tracker not moving through both maximum load points at the same time.

These measurements conclusively show that the power consumption when the system is not moving to be just less than half a Watt and when the system is moving both axes in a worst-case scenario, it consumes 5.52 W.

4.1.3 Comparison to Other Systems

The final part of the functionality testing of the tracking system is to compare its performance to other types of panel orientations and tracking systems. To do this, an accurate simulation of the sun's angle to particular point on the earth's surface was needed to calculate the power and energy gained by a tracking system.

To simplify the math, a few assumptions were made. One is that the earth is perfectly spherical so that elevation of the solar panel setup does not come into play. Second is assuming that the sun moves from exactly east to exactly west every day of the year. Finally, that the year is exactly 365, 24 hour days or 8760 hours long. Finally, that the time at the point of the solar panel corresponds to the sun's position so that at midnight the sun is exactly behind the earth at 180° to the zenith and that at noon, the sun is directly between the east and west horizons or 0° to the zenith.

Given that the earth rotates a full 360° in 24 hours in an east-to-west direction, the following equation can be given for the angle of the sun to the zenith of the point on the earth given in the east-west direction henceforth called the X direction:

$$Z_X = 15° (t - 12)$$

The variable t is the amount of time from midnight on the first day of the simulation in hours. This equation gives the following results:

t = 0 hours (midnight first day),	$Z_X = 15°(-12) = -180°$
t = 12 hours (noon first day),	$Z_X = 15°(0) = 0°$
t = 24 hours (midnight second day),	$Z_X = 15°(12) = 180°$
t = 36 hours (noon second day),	$Z_X = 15°(24) = 360° = 0°$

And the cycle repeats every day.

To find an equation for the sun in the north-south direction, henceforth referred to the Y direction, the tilt of the earth's axis to its orbit around the sun is given at 23.5°. So as the earth orbits around the sun, the equator's Y angle to the sun goes from 0° at the vernal equinox to 23.5° at the summer solstice back to 0° at the autumnal equinox then to -23.5° at the winter solstice and finally back to 0° at the vernal equinox again. Given that this value fluctuates over the 365 day or 8760 hour year, the angle to the zenith on the equator is given as:

$$Z_{Yequator} = 23.5°\sin\left(\frac{2\pi}{8760}\, t\right)$$

The time variable t is now the measure of hours from the midnight on the vernal equinox. However, because the point chosen might not be at the equator, the latitude also comes into effect. Positive latitude is the angle of the point specified on the earth's surface north of the equator. Negative latitude is consequently south of the equator. So to bring the latitude into the equation, Z_Y is now the difference of the latitude angle, defined as Φ, to the angle of the sun to the equator:

$$Z_Y = \Phi - 23.5° \sin\left(\frac{\pi}{4380}\, t\right)$$

Now that equations for the X and Y angle of the sun to the zenith of some point on the earth have been derived, the amount of available sunlight radiation to that point can be calculated. NASA defines this amount of radiation under perfectly sunny and clear conditions to be a function of the cosine of the angle of the sun to the zenith [11]. So the radiation percent coming from both individual directions is defined as:

$$R_X = \cos(Z_X) = \cos(15° (t - 12))$$

$$R_Y = \cos(Z_Y) = \cos(\Phi - 23.5° \sin(\frac{\pi}{4380} t))$$

And then the total radiation of the sun hitting a point on the earth's surface at latitude Φ at time t in hours from midnight on the vernal equinox is:

$$R_T = R_X * R_Y = \cos(15° (t - 12)) * \cos(\Phi - 23.5° \sin(\frac{\pi}{4380} t))$$

Putting this equation into MATLAB and plotting the radiation hitting Worcester, Massachusetts which is Φ = 42.2625° north over a 24 hours starting on the midnight of the vernal equinox and discarding all negative values yields this graph:

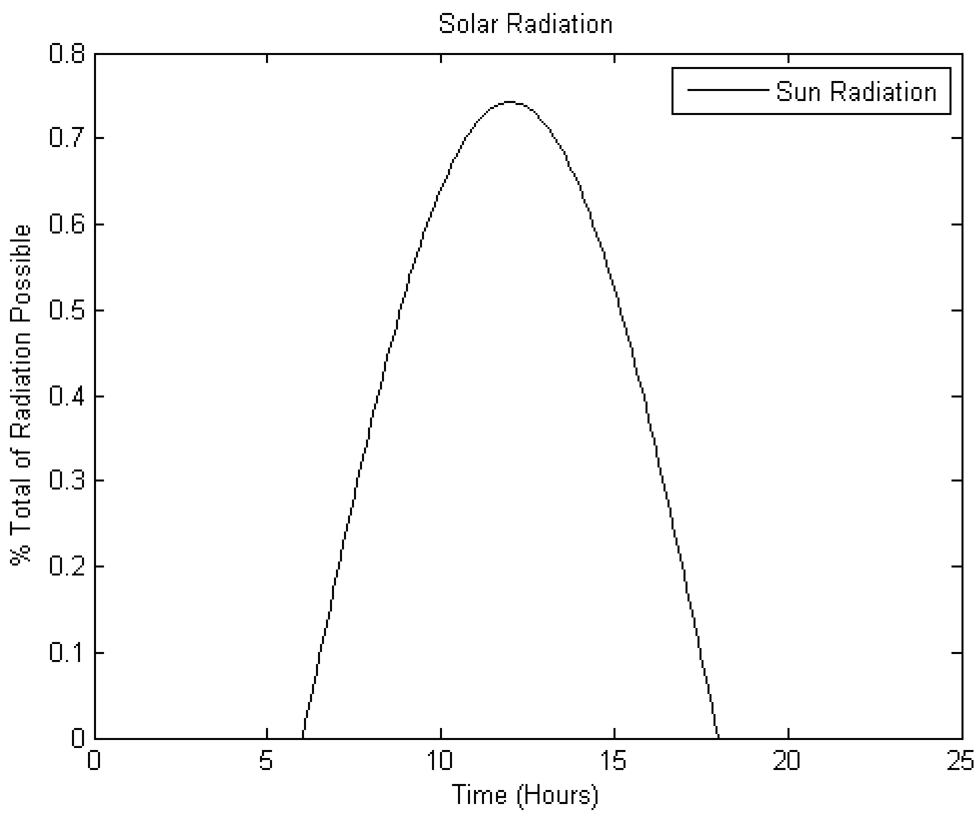

Figure 33: Percent Total Solar Radiation in Worcester, MA on the Vernal Equinox

Notice how the percent of the radiation never reaches 100%. This is because the sun is off by 42.2625° from Worcester on the vernal equinox.

To ensure that the angle Z_Y is changing correctly, the plot time was widened to a full 365 day, 8760 hour year and the following plot was produced:

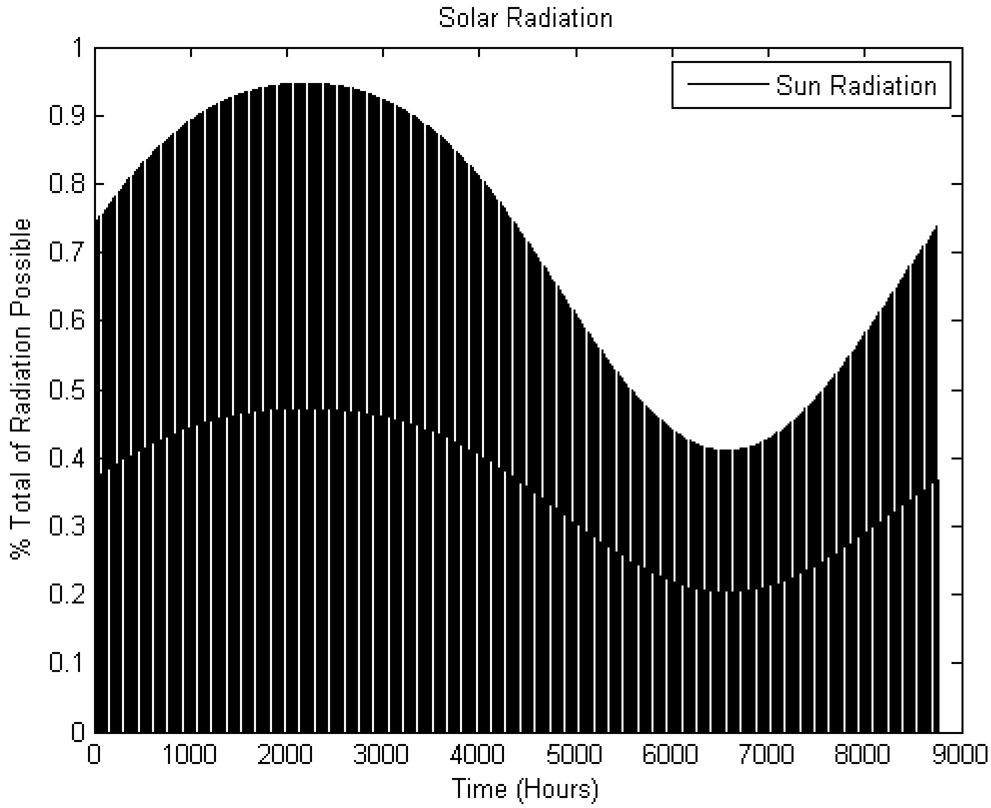

Figure 34: Percent Total Solar Radiation in Worcester over a Year in Worcester, MA

The solidity of the plot is due to the fact that the radiation is oscillating every day and there is 365 days' worth of data in the above plot. However, it does show that the percent total varies over the year as well as over the day and returns to the same point as it began verifying the equation for Z_Y. Also, the percent again never reaches 100% again because Worcester has latitude greater than 23.5° so the sun can never be directly overhead.

To calculate the percent radiation absorbed by the solar tracking system, several observations are made about the movement of the tracker. The first is that the tracker will always be following the sun slightly behind its actual position by a maximum of 1.5° in both directions as verified by the measurements. Taking the cosine of this angle shows that the tracker will be able to absorb 99.97% of all available light in one direction. For both directions, this vale is squared bringing the percentage to 99.93% of all available radiation in both directions. Second is that aside from this error, the tracker will always orient any solar panel on it perpendicular to the sun in perfectly clear conditions.

Therefore, based on these assumptions the radiation absorbed by a panel mounted on this tracking system will be 99.93% of the total radiation meaning that the equation for this value over time will be:

$$P_{DT} = 0.9993 * R_{Total}$$

$$P_{DT} = 0.9993 * \cos(15° (t - 12)) * \cos(\Phi - 23.5° \sin(\frac{\pi}{4380} t))$$

Before plotting the equation for the dual tracker system over time, equations for several other systems needed to be derived for comparisons. The first being the tracker that only tracks in the east-west or X direction which is also referred to as a Horizontal Single Axis Tracker (HSAT) as discussed in Chapter 2. First, assuming the HSAT uses the same tracking system as the dual axis tracker, the tracking angle will lag slightly behind the sun by 1.5° over the course of a day. This means in the X direction, the HSAT can only absorb 99.97% of the radiation available. Second the HSAT will be oriented in the Y direction so it is pointed towards the zenith. Therefore, the HSAT percentage absorbed will also rely on the angle of the sun in the Y direction which it cannot compensate for. The absorption percent will be affected the cosine of Z_Y which brings the total equation to:

$$P_{XT} = 0.9997 * \cos(Z_X) * R_{Total}$$

$$P_{XT} = 0.9997 * \cos^2(15° (t - 12)) * \cos(\Phi - 23.5° \sin(\frac{\pi}{4380} t))$$

Tracking can also be done in the Y direction. This is usually done by using an immobile panel and varying its degree to zenith over the year to keep the sun's angle to the panel minimal without any mechanics. To simplify the mathematics and make the comparisons more relevant, two things are assumed. First, the tracker, man or machine, has the same amount of error in the Y direction as the HSAT tracker has in the X direction which is 99.97%. Second the panel is oriented in the X direction towards the zenith in the same way that the HSAT is oriented in the Y direction. Therefore, the Y direction tracker percentage absorbed will also rely on the angle of the sun in the X direction which the tracker cannot compensate for. The absorption percent will be affected the cosine of Z_X which brings the total equation to:

$$P_{YT} = 0.9997 * \cos(Z_Y) * R_{Total}$$

$$P_{YT} = 0.9997 * \cos(15° (t - 12)) * \cos^2(\Phi - 23.5° \sin(\frac{\pi}{4380} t))$$

The final panel orientation to be compared is the immobile panel orientation. This is assuming that the panel is placed perfectly level with the ground so that the panel's normal is perfectly oriented to the zenith. Therefore the percent of radiation absorbed with an immobile panel will be a function of the angle of the sun in both directions. This value will be determined by the cosines of both Z_X and Z_Y which brings the equation to:

$$P_{YT} = \cos(Z_X) * \cos(Z_Y) * R_{Total}$$

$$P_{YT} = \cos^2(15° (t - 12)) * \cos^2(\Phi - 23.5° \sin(\frac{\pi}{4380} t))$$

After deriving all four equations, they were used in MATLAB to create vectors over time during the day of the vernal equinox. Plotting the results returned the following graph:

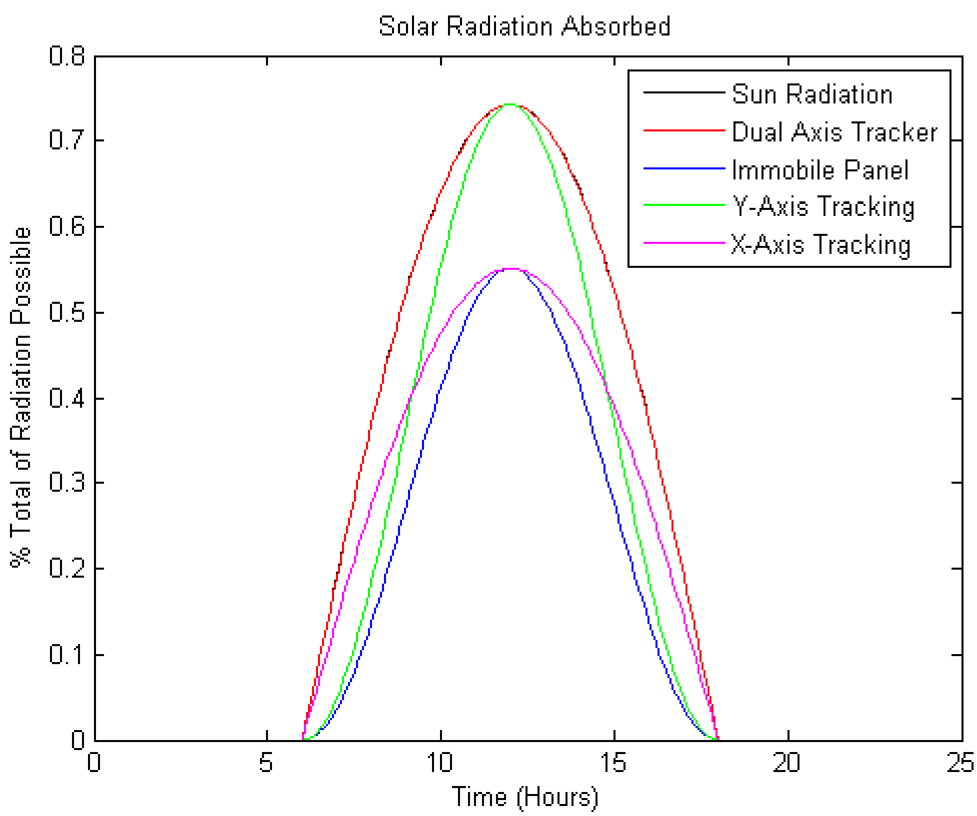

Figure 35: Solar Radiation Absorption Percentages in Worcester, MA on the Vernal Equinox

First of all, the graph clearly shows that the dual-axis tracking system, despite its error, is absorbing almost all the available light. The X-axis tracking seems to be the better tracking system at the beginning of the day, when the sun is first rising but after a few hours it falls behind the radiation absorbed by the Y-axis. This is because the X-axis still suffers from the fact that it is pointed towards the zenith in the Y direction and will never be able to achieve the high percent absorption that the Y-axis benefits from at noon. Finally, the immobile tracker clearly has the least amount of absorption as it cannot compensate for its error in either direction.

This graph shows the absorption over a single day over a whole year, the results might be a little different. Because plotting over a full year will result in an indecipherable like in Figure 34, this action was avoided. However, taking the integral of the power absorbed over a full year will provide a figure for energy gained as well as a metric for comparing the benefits of a tracking system over a full year.

To do this, a few more assumptions were made. First was that over the full year, the days remained cloudless, clear and had perfect atmosphere conditions for transferring sunlight. This means that according to NASA, the sun is outputting approximately 1 kW/m^2 to the earth's surface when the radiation percentage is 100% [11]. Second, the panel mounted to each tracking setup is perfectly identical and has a power absorption and production of is also 1 kW/m^2. The reason for this being is twofold. One is to simplify the mathematics by not requiring a change in any of the above equations and second is because when comparing two types of tracker, the value drops out and becomes irrelevant anyways.

However, integrating the equations becomes an issue as the equation includes the following statement:

$$\cos(\Phi - 23.5° \sin(\frac{\pi}{4380} t))$$

This cannot be integrated or reduced to elementary mathematical terms. Furthermore, attempts to integrate the value over a definite integral using Mathematica resulting in a long period of waiting followed by a program crash. Because the discrete data points for the previous simulation were already available in MATLAB, the values were approximated by summation.

Approximating by summation means that MATLAB is summing all the data points across the entire simulated year and then multiplying by the step size which was a fraction of an hour. Doing the same calculations over progressively smaller step sizes resulted in the following values which are all in kWh:

Step Size	Total Available	No Tracking	X-Axis Tracking	Y-Axis Tracking	Dual-Axis Tracking
1 hour	1966.998538	1182.619107	1497.102311	1552.821624	1965.818516
1/10 Hour: 6 minutes	1977.647205	1182.619047	1505.25575	1552.821543	1976.460795
1/100 Hour: 36 seconds	1977.707068	1182.619046	1505.305588	1552.821542	1976.520622
1/1000 Hour: 3.6 seconds	1977.707106	1182.619046	1505.305609	1552.821542	1976.520659

Table 5: Simulated kWh Generated by Tracking Systems over a Year in Worcester, MA

Here, the difference between the $1/100^{th}$ step size and the $1/1000^{th}$ step size is practically null so the results from the $1/1000^{th}$ step size are taken to be an adequate approximation of the integral. The MATLAB code used to produce all these values is included in Appendix G.

However, each tracking system uses a certain amount of power over the entire year to track the sun at that degree of precision. Based on the measurements in the previous section, the dual-axis tracker consumes 5.52W during movement and a single axis would use at worst, 3.6W. Otherwise it is consuming 0.48W at standby. As shown in the simulation in chapter 3, the tracker moves once every 7 seconds for one millisecond. Each time lasting only one millisecond means that dual-axis tracking consumes 5.52 mWs every time it moves single-axis tracking consumes 3.6 mWs. Multiplying out the 7 second interval time, this means that the tracker moves approximately 6180 times over 12 hours of sunlight. Again multiplying the values moving the dual-axis tracker consumes 34.2 Ws over the course of a day with 12 hours of sunlight which means it consumes just under 0.01 Wh a day or 0.00345 kWh a year. Doing the same calculations for the single-axis tracker returns the values of 22.3 Ws which is under 0.007 Wh a day or 0.00256 kWh a year. This is an almost negligible value when the tracker is consuming 0.48W for all 24 hours of the day meaning it consumes 11.52Wh a day or 4.205 kWh a year.

These calculations mean that the net energy gain for the dual axis tracking system is 4.20845 kWh less and the single-axis trackers are 4.20756 kWh less. To get the approximate energy gained by tracking, a model solar panel is picked to make the comparisons. A 20W solar panel is chosen for this comparison because its size and weight are right around the expect load limit on the mechanical construction of the tracker. This is assuming that the weight of the solar panel is compensated by a counterweight so the mechanical load to the motor has remained the same. 20 Watts signifies that at maximum solar radiation, which is what was calculated above, 0.02 of that is converted into electrical energy. So the energy produced by the tracker systems is multiplied by 0.02 and then the appropriate value of energy consumed over the year is calculated:

	No Tracking	X-Axis Tracking	Y-Axis Tracking	Dual-Axis Tracking
Net Energy Generated (kWh)	23.65238	25.81440	26.76472	35.23779

Table 6: Net Energy Generated by 20W Tracking Systems over a Year in Worcester, MA

With the net energy calculations, the systems can be compared numerically by using the net energy gain over using just the immobile solar panel. The numbers used are from the 1/1000th step size results and all results in this table are assuming perfectly ideal conditions over the entire year and each system is using the same identical 20W solar panel:

	% Gain over Immobile	% Gain over X-Axis	% Gain over Y-Axis
X-Axis Tracking	9.141%	-	-
Y-Axis Tracking	13.159%	3.681%	-
Dual-Axis Tracking	48.982%	36.504%	31.658%

Table 7: Percent Gains of Tracking Systems over a Year in Worcester, MA

Here, the clear advantage goes to the dual-axis tracker which offers over a 48% energy gain over the exact same solar panel in an immobile setup. Dual-axis tracker also shows a large difference in energy gained over single-axis tracking with over a 30% gain in both setups.

Table 7 also makes it apparent that for Worcester’s latitude, a Y-Axis tracker overs a larger amount of energy generated over the X-Axis tracker. But this advantage decreases and eventually disappears when the tracker's placement gets closer and closer to the equator. To represent this graphically, the same MATLAB program that was used to generate the energy measurements for the year was run over all latitudes and then plotted the energies generated over the latitude of the tracker's placement. Below are the results:

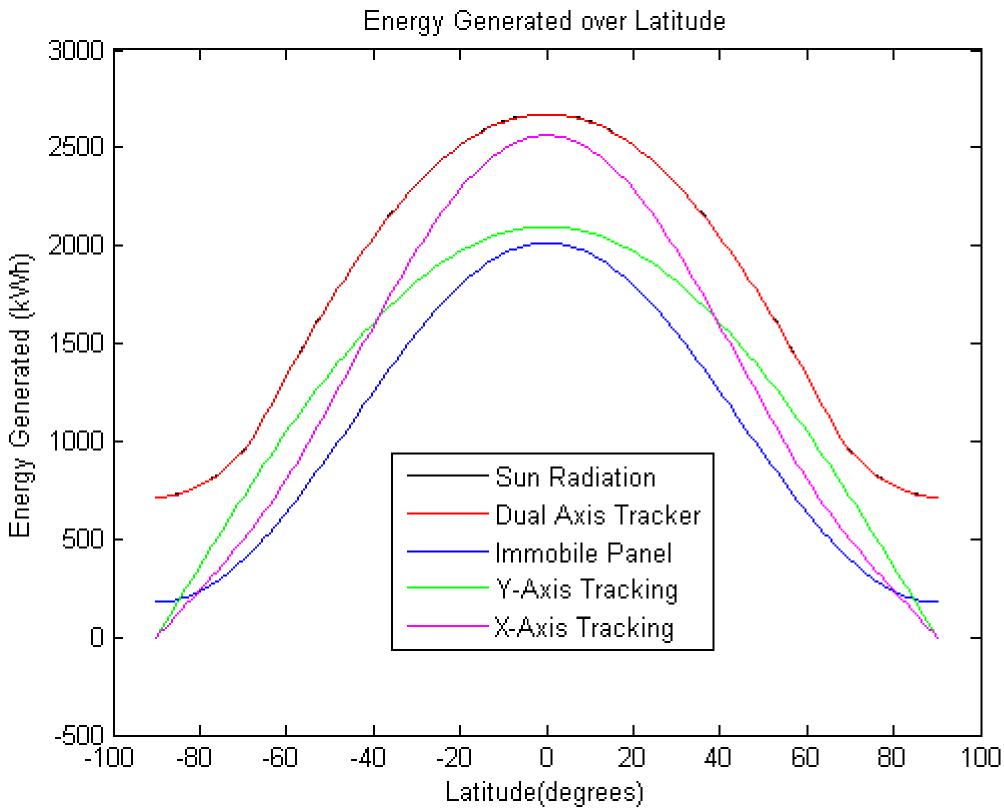

Figure 36: Energy Generated over a Range of Latitudes

This graph clearly shows that near the equator, the X-Axis tracker has a greater amount of energy generated over the Y-Axis tracker. However, farther from the equator, the Y-Axis tracker has the larger energy generated. The point at which the two cross is right around the latitude of 40°. The exact point cannot be calculated without the equation for the energy generated.

Furthermore, this graph shows that the dual-axis tracker outlined in this report generates more energy than Y-Axis trackers, X-Axis trackers or immobile panels across the entire surface of the planet. The MATLAB code used to generate this data is included in Appendix H.

4.2 Cost Analysis

Although a tracker might be highly efficient and provide a good average energy gain compared to an immobile system or a single axis system, this is not enough yet to claim the system is beneficial over its alternatives. The added tracking component to the system must provide enough power gain that there is either an immediate payback or the payback period is less than the lifetime of the system. Thus the initial cost of the system, the lifetime, and the payback period need to be found to determine the cost effectiveness of the tracker system.

The total cost of the project was $436.45, but this included all the material for testing and the initial prototypes. The final prototype by itself cost $333.99, which did not include shipping. However, the final prototype did not benefit from the cheapest industrial prices. Thus a cost summary was done for an estimated 1,000 units. The prices values were taken from several component distributers. The list of parts used and the respective prices can be seen in Table 8. The overall price for a single tracker, cost $315.15. Shipping and handling were once again not included.

Quantity x 1000	Part Description	Manufacturer	Unit Price	Cost
20,000	0.125" Thick Acyrlic - per square inch	US Plastic	$97.44	$487.20
88,000	0.25" Thick Acyrlic - per square inch	US Plastic	$181.60	$3,632.00
175,000	0.5" Thick Acyrlic - per square inch	US Plastic	$397.25	$15,095.50
32,000	4-40 + 6-32 x 1/4" (Philips and Flathead)	Stock Drive	$4.15	$1,328.00
2,000	9V Battery Holder	Mouser	$0.63	$1,262.00
13,000	0.25" Diameter Brass Rod - per inch (length)	Metals Depot	$19.32	$1,758.12
4,000	0.375" Diameter Brass Rod - per inch (length)	Metals Depot	$34.08	$954.24
2,000	3.76" Worm Gear, 180 Teeth, Bronze	Stock Drive	$48.50	$97,000.00
2,000	0.75" Worm, Steel	Stock Drive	$10.71	$21,420.00
12,000	Acrylic Parts, Rubber Feet, Metal Mounts, etc.	Stock Drive	$1.50	$18,000.00
10,000	Assorted Sized Nuts	Stock Drive	$8.97	$897.00
2,000	Set Screws (Torx)	Stock Drive	$5.74	$114.80
8,000	Standoffs less than 10-32	Mouser	$0.70	$5,600.00
13,000	Assorted Sized Washers	Stock Drive	$3.97	$516.10
16,000	22 gauge solid wire (assorted colors) - per foot	Digikey	$13.07	$2,090.88
8,000	1.5V Battery	Mouser	$0.47	$3,760.00
2,000	12 V DC Motor	Surplus Trader	$2.09	$4,180.00
1,000	Large DSPT Toggle Switch	Mouser	$3.34	$3,340.00
1,000	Arduino Microcontroller	Arduino	$29.95	$29,950.00
1,000	Parts for PCBs	Mouser	$30.56	$30,560.00
2,000	Protoboards	Advanced Circuits	$33.00	$66,000.00
4,000	1.5V 135mA Solar Cell	Futerlec	$1.80	$7,200.00
			Total	**$315,145.84**
			One Tracker	**$315.15**

Table 8: Cost of AADAT

To reduce the cost significantly, several of the parts can be replaced and/or removed. Two significant alterations that impact the cost is the microcontroller and gear/motor setup. The Arduino houses the ATMega 328P microcontroller, which can be replaced by any one of the Atmel AVR family including the ATMega 8 which can be bought singularly from Digikey for $2.11 per unit for a thousand units. This chip along with a 16 Mhz oscillator crystal, a 12 V to 5 V regulator, and a few other components can replace the entire Arduino for roughly $3.00 per tracker. This in turn reduces the tracker cost down to $288.55. Additionally, the DC motor used can be replaced with a geared motor assembly. Models ranging from 1, 30, and 60 RPM are available from digikey for $30.63 per unit for 500 units. This change decreases the tracker cost to $227.21.

The lifetime of the system is determined by the element that has the highest likelihood to fail, which is the motor. An average DC motor used for light loads, below 30Amps/in^2, has a lifetime from 720-2,000 hours [11]. To use a specific number, the midpoint of 1375 hours is used. It was assumed that daylight exists for 12 hours of a day and the tracker moves every 7 seconds for a half second, based on calculations in Section 3.3.1. This means that in a day the tracker moves for about 2880 seconds. In a year it will move for about 292 hours. Thus the motor has a lifetime of about 4 years.

The US Energy Information Administration calculated that about 11,040 kWh of electric energy is consumed on average by an American household within a year. An assumed energy goal from solar energy of 25% of the total means a required 2,760 kWh produced in a year. One calculator (alstore.com) predicts that 12 panels at 200 Watts would be required, a total of 2,400 Watts. Assuming an ideally mounted immobile system, about 70% of the radiation would be absorbed. Based on the background the tracker system would allow for 95% of radiation. If these percentages are used as a multiplier, then the resulting power would be roughly 1,680 Watts and 2,280 Watts. This means that an extra six panels are required for the immobile system, while only one extra panel is required for the tracker system.

Immobile: (2,400-1,680)/(200x0.7) = 5.14 panels

Tracker: (2,400-2,280)/(200x0.95) = 0.63 panels

This results in a 50% increase in price on solar panels for the immobile system, while only an 8% increase in price for the tracker system.

Finally, the payback period for a 20 Watt solar panel is calculated. Four scenarios are considered; the solar panel is immobile, an X-axis tracker is used, a Y-axis tracker is used and the AADAT designed is used. In Massachusetts the US Energy Information Administration calculated the electricity rate was 15.29 cents per kWh. It is assumed this value is also the payback price. A 20 Watt solar panel from HQRP.com can be bought for $108.92. The payback period for the immobile system versus the AADAT system were compared for solar panels from one to twenty 20 Watt panels. This data can be seen in Appendix G and the results are seen in Figure 37. For four 20 Watt solar panels the payback period of the AADAT system is 30.76 years while it is 30.13 years for the immobile system. At twenty panels the payback period is 22.33 years for the AADAT system, while it is constant at 30.12 years for the immobile system.

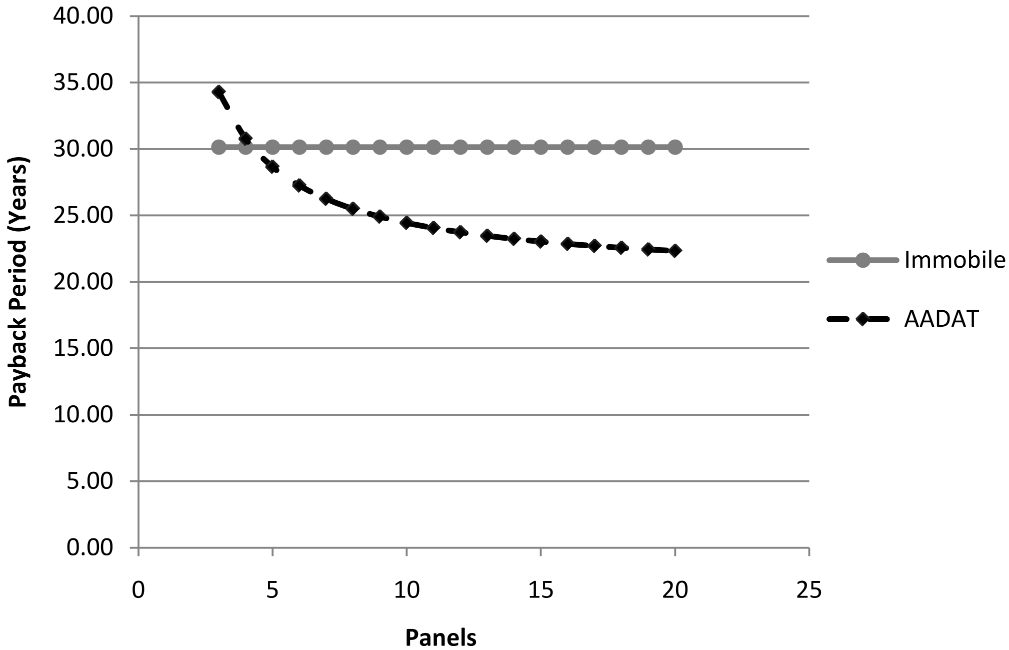

Figure 37: Payback Periods for Immobile versus AADAT

4.3 Observed Drawbacks

The AADAT has a few observed drawbacks. Many of these drawbacks were a result of limited research available for certain design parts as well as limited resources. The four most significant sections that could have benefited from more research were the overall mechanical design, the sensor array, the microcontroller and the power supply.

This project was designed and constructed by two electrical engineering students, with no aid from a mechanical engineer. This resulted in a functional mechanical setup, but one that has a few significant problems. One problem was the cost; the gears cost a total of $118.42, which was 37% of the cost. Another problem was that no stress analysis was done on any part of the system and the gears are not perfectly aligned to reduce friction. This results in increased stress and could result in a long-term failure of the system.

For the sensor array only two types of sensors were tested: photoresistors and photovoltaics. Also only the tilted mount array was tested and used in the tracker. One disadvantage to using the photovoltaics is even at the optimum tilt angle, they did not provide fully linear responses. The disadvantage to using the tilt array is that if a light source besides the sun was in the vicinity it could confuse the tracker and possibly misalign the tracker.

The Arduino AVR development board was primarily used due to its high-speed prototyping ability and availability. However, as mentioned earlier, the microcontroller chip used in the Arduino was all that was needed to create a functional tracking system and is a lot cheaper. Also the microcontroller does not have any algorithm to account for clouds or other obstructions. This can lead to misalignment of the tracker and significant angular error due to shadows.

The last known section that had drawbacks was the power supply. The eight 1.5 V AA batteries used provided the needed 12 V, but had poor capacity. The batteries had to be replaced after about two weeks of testing. When the batteries were significantly discharged the motors stopped working and the system did not function. In actual use this could result in major loss of power generated and, possibly even generate less than an immobile system.

5 Conclusion and Future Considerations

The completion of this project has led to several conclusions to be made about this solar tracking system as well as solar tracking systems in general. Several recommendations were also outlined for future consideration in the continuing development of solar tracking systems

5.1 Conclusions

The Azimuth-Altitude Dual-Axis Solar tracker designed and built in this project show a clear benefit over both immobile and single-axis tracking systems. The tracker built has a maximum angular error to the sun of 1.5° in both axes of movement. This value corresponds to a 49% energy gain over an immobile solar panel setup assuming the solar panels mounted on the tracker and the immobile system are identical 20W panels. Furthermore, the single-axis trackers had gains over the immobile system for the entire range of latitudes but these gains were still lower than the dual-axis tracker for all latitudes.

Furthermore, testing showed that the power used by the tracking system built was much less than the power gained by tracking the sun accurately. This means that if the tracking system were to charge its own batteries, it would be entirely self-sufficient except for maintenance.

Perhaps the most important conclusion to be made from this project is the total cost for this tracking system is very low, less than $300 in parts for each tracker in mass quantities. This means that the system can be built for a very low cost and most importantly; this system would be within the financial reach of many developing country communities. Based on the simulations, test results and cost analysis this project has met its original goals. To improve the efficiency of this tracking system, however, this project has several future recommendations for future study in solar trackers.

5.2 Future Considerations

As stated by section 4.3, there are a few disadvantages to the tracker. However, many of these disadvantages can be accounted for with a few adjustments in the design. The four areas of adjustment are the mechanical system, the sensor array, the power supply, and microprocessor functionality.

5.2.1 Different Mechanical Adjustments

The mechanical system in the future should be designed and analyzed properly in simulation software such as CAD. This should be done by an experienced mechanical engineer who would be able to quickly determine errors and poor mechanical design. Aside from mechanical design adjustments, the motor/gear system should be changed. There are three possible alternatives: a stepper motor, a further geared motor, or hydraulics. Both the stepper motor and further geared motor provide a significant decrease in the overall cost. Hydraulics might be better in power efficiency when moving large panel arrays, but it is uncertain if it would decrease cost. Finally, all the materials for the bearings and mechanical connections should be investigated by a materials engineer for outdoor use and altered accordingly.

5.2.2 Solar Array Variations

There are a variety of solar sensors that were never tested or implemented. This primarily includes photodiodes and phototransistors, but also includes different photoresistors and photovoltaics. Further investigation in the dimensions and the spacing between the sensors should be conducted. Further investigation should also be done with the divider mount and the mount with a collimator for the sensors. One observation made was that perhaps only three sensors are required using a microcontroller with a specialized geometric algorithm.

5.2.3 Power Supply Improvements

The power supply is not ideal for actual production. Ideally a battery would be used that is highly available in an unprivileged country, such as a small sealed lead acid or car battery. This battery could be utilized twofold as a power source for the tracker and to store the power from the solar panel(s) connected to the tracker. The use of the battery to store energy would require the design of a robust charging system. In addition this system should ideally integrate a maximum power point tracker (MPPT) and perhaps even incorporated into the same microcontroller being used for tracking to reduce the cost of adding this feature. MPPT is an efficient DC to DC convertor, which allows for the maximum power to be taken from the solar panel(s) at any moment in time. Research should be focused on designing an MPPT and finding the most suitable battery.

5.2.4 Additional Microprocessor Functionality

The microprocessor functions used are quite simple and only pertain to nominal conditions. As mentioned earlier, clouds and obstructions can result in major misalignment. One way to improve this error would be to calculate the approximate position of the sun using a location and time-based algorithm and then using the sensor array to reduce the error to a minimum. A second way to solve this error is to only check the angle of the sun and adjust the tracker once every few minutes or so. Another possible function that the microcontroller could provide is the auto-calibration of the solar sensors. As shown in testing, miscalibrated sensors can result in either poor tracking or the system not reaching a state of equilibrium. This can be implemented by using internal compensation through programming or digitally controlled potentiometers for external compensation.

6 References

[1] Bailis, Robert. “Wood in Household Energy Use”. *Encyclopedia of Energy*. 2004. Pages 516, & 518.

[2] Ackermann, T., Andersson, G., Söder, L. “Distributed generation: a definition”. *Electric Power Systems Research*. April 2000. Page 195.

[3] Banerjee, “Comparison of Options for Distributed Generation in India”. *Energy Policy*. Pages 105-110.

[4] Goetzberger, A., Hebling, C., Schock, H.. “Photovoltaic materials, history, status and outlook”. *Materials Science and Engineering: R: Reports*. 2002.

[5] Mousazadeh, H., Keyhani, A., Javadi, A., Mobli, H., Abrinia, K., Sharifi, A.. “A review of principle and sun-tracking methods for maximizing solar systems output”. *Renewable and Sustainable Energy Reviews*. January 2009. Pages 1800, 1800, 1804, 1806, & 1812.

[6] Krauter, Stefan. “Solar Electrical Power Generation: Photovoltaic Energy Systems”. Springer. 2006. Pages 21-22.

[7] Mehleri, E., Zervas, P., Sarimveis, H., Palyvos, J., Markatos, N.. “Determination of the optimal tilt angle and orientation for solar photovoltaic arrays”. *Renewable Energy*. April 2010. Page 2469.

[8] Sefa, I., Demirtas, M., Çolak, I.. “Application of One-Axes sun Tracking System”. *Energy Conversion and Management*. 2009. Page 2710.

[9] Poulek, V., Libra, M.. “A Very Simple Solar tracker for Space and Terrestrial Applications”. *Solar Energy Materials and Solar Cells*. 2009. Pages 99-101.

[10] Roth, P., Georgiev, A., Boudinov, H.. “Cheap two Axis sun Following Device”. *Energy Conversion and Management*. 2005. Page 1180.

[11] Stickler, G., Kyle, L.. "Educational Brief Subject: Solar Radiation and the Earth System". National Aeronautics and Space Administration. <http://edmall.gsfc.nasa.gov/inv99Project.Site/Pages/science-briefs/ed-stickler/ed-irradiance.html>

[12] Hamilton, R. “DC Motor Brush Life”. IEEE Transactions on Industrial Applications. 2000. Page 1687.

Appendix A: Motor PSPICE Simulation

The following PSPICE code was used to simulate the motor.

```
* MQP_Motor

VS 1 0 12
RM 1 2 2.19
LM 2 3 1.057m
EM 3 4 VALUE={0.0212*I(VF)}
VD 4 0 0

ET 10 0 VALUE={0.0212*I(VD)}
RA 10 11 1u
ER 11 12 VALUE={0.0025*PWR(I(VF),0.088)}
LJ 12 13 0.00001
VF 13 0 0

.PROBE
.IC V(1) = 0
.TRAN 0 0.30 1m UIC
.END
```

Appendix B: Sensor Data

This is the data for the photosensors tested.

Photoresistors:

θ	Difference (25°)	V difference (35°)	Difference (45°)	V Difference (55°)	V Difference (65°)
0	0.023	0.018	0.009	0.004	0.005
5	0.074	0.055	0.033	0.015	0.014
10	0.122	0.090	0.053	0.022	0.020
15	0.166	0.132	0.072	0.031	0.026
20	0.219	0.206	0.117	0.045	0.036
25	0.248	0.246	0.164	0.057	0.045
30	0.284	0.281	0.241	0.078	0.056
35	0.313	0.311	0.295	0.105	0.074
40	0.345	0.340	0.323	0.141	0.094
45	0.370	0.365	0.350	0.201	0.123
50	0.387	0.382	0.362	0.263	0.172
55	0.392	0.387	0.368	0.302	0.212
60	0.396	0.390	0.370	0.321	0.270
65	0.398	0.389	0.370	0.326	0.296
70	0.399	0.389	0.368	0.321	0.300
75	0.399	0.388	0.366	0.317	0.294
80	0.398	0.386	0.362	0.309	0.278
85	0.396	0.383	0.359	0.301	0.262
90	0.395	0.381	0.355	0.291	0.237
0	0.020	0.017	0.009	0.004	0.005
-5	-0.010	-0.003	-0.005	-0.002	0.000
-10	-0.048	-0.027	-0.020	-0.011	-0.006
-15	-0.106	-0.065	-0.049	-0.021	-0.014
-20	-0.179	-0.109	-0.075	-0.032	-0.020
-25	-0.269	-0.164	-0.106	-0.043	-0.027
-30	-0.332	-0.283	-0.176	-0.064	-0.040
-35	-0.360	-0.334	-0.255	-0.087	-0.050
-40	-0.381	-0.367	-0.322	-0.132	-0.068
-45	-0.392	-0.382	-0.351	-0.181	-0.090
-50	-0.401	-0.390	-0.364	-0.253	-0.119
-55	-0.403	-0.393	-0.370	-0.288	-0.167
-60	-0.403	-0.393	-0.371	-0.306	-0.224
-65	-0.401	-0.392	-0.371	-0.313	-0.258
-70	-0.398	-0.389	-0.369	-0.315	-0.279
-75	-0.395	-0.384	-0.366	-0.313	-0.285
-80	-0.389	-0.378	-0.360	-0.306	-0.278
-85	-0.383	-0.372	-0.355	-0.296	-0.265
-90	-0.377	-0.364	-0.347	-0.282	-0.240

Thin Film Photovoltaics:

θ	Difference (25°)	V difference (35°)	Difference (45°)	V Difference (55°)	V Difference (65°)
0	-0.063	-0.132	-0.136	-0.218	-0.200
5	0.289	0.110	0.039	-0.135	-0.124
10	0.583	0.331	0.166	-0.087	-0.071
15	0.913	0.568	0.250	-0.015	-0.032
20	1.194	0.966	0.453	0.070	0.040
25	1.326	1.240	0.697	0.138	0.108
30	1.472	1.406	1.071	0.238	0.190
35	1.574	1.520	1.404	0.360	0.278
40	1.687	1.613	1.541	0.516	0.394
45	1.766	1.702	1.654	0.748	0.555
50	1.804	1.743	1.681	1.069	0.792
55	1.821	1.754	1.686	1.300	1.065
60	1.822	1.750	1.677	1.430	1.294
65	1.816	1.741	1.663	1.454	1.376
70	1.807	1.723	1.634	1.431	1.364
75	1.791	1.707	1.606	1.397	1.330
80	1.771	1.682	1.577	1.351	1.276
85	1.759	1.662	1.545	1.306	1.220
90	1.744	1.647	1.515	1.262	1.158
0	-0.071	-0.127	-0.139	-0.212	-0.205
-5	-0.267	-0.265	-0.229	-0.270	-0.245
-10	-0.482	-0.405	-0.341	-0.338	-0.294
-15	-0.760	-0.635	-0.456	-0.411	-0.355
-20	-1.053	-0.812	-0.553	-0.470	-0.394
-25	-1.150	-0.980	-0.655	-0.515	-0.433
-30	-1.134	-1.115	-0.862	-0.592	-0.491
-35	-1.195	-1.186	-1.018	-0.671	-0.544
-40	-1.259	-1.242	-1.140	-0.794	-0.606
-45	-1.290	-1.263	-1.184	-0.919	-0.675
-50	-1.307	-1.282	-1.205	-1.030	-0.736
-55	-1.310	-1.282	-1.208	-1.063	-0.795
-60	-1.306	-1.272	-1.198	-1.057	-0.867
-65	-1.299	-1.253	-1.184	-1.036	-0.887
-70	-1.273	-1.228	-1.154	-1.000	-0.866
-75	-1.253	-1.200	-1.124	-0.953	-0.827
-80	-1.214	-1.158	-1.070	-0.868	-0.713
-85	-1.180	-1.116	-1.022	-0.788	-0.597
-90	-1.130	-1.060	-0.969	-0.682	-0.442

Polycrystalline Photovoltaics:

θ	Difference (25°)	V difference (35°)	Difference (45°)	V Difference (55°)	V Difference (65°)
0	0.017	0.023	0.024	0.008	0.030
5	0.130	0.109	0.074	0.037	0.056
10	0.209	0.166	0.112	0.056	0.074
15	0.306	0.225	0.146	0.074	0.090
20	0.434	0.332	0.207	0.103	0.117
25	0.474	0.425	0.271	0.122	0.134
30	0.502	0.491	0.361	0.157	0.169
35	0.510	0.511	0.448	0.195	0.208
40	0.522	0.527	0.496	0.237	0.252
45	0.528	0.535	0.509	0.297	0.314
50	0.536	0.538	0.516	0.363	0.389
55	0.543	0.540	0.517	0.429	0.437
60	0.550	0.544	0.515	0.455	0.454
65	0.558	0.547	0.514	0.459	0.452
70	0.567	0.549	0.511	0.451	0.439
75	0.575	0.552	0.508	0.437	0.420
80	0.574	0.547	0.501	0.418	0.393
85	0.561	0.537	0.490	0.400	0.362
90	0.549	0.524	0.476	0.380	0.328
0	0.021	0.022	0.027	0.006	0.031
-5	-0.047	-0.022	0.000	-0.011	0.017
-10	-0.144	-0.086	-0.041	-0.035	-0.002
-15	-0.273	-0.183	-0.100	-0.064	-0.027
-20	-0.336	-0.269	-0.158	-0.091	-0.048
-25	-0.380	-0.365	-0.214	-0.120	-0.067
-30	-0.438	-0.445	-0.322	-0.162	-0.104
-35	-0.478	-0.482	-0.421	-0.212	-0.136
-40	-0.540	-0.533	-0.501	-0.307	-0.195
-45	-0.574	-0.562	-0.534	-0.398	-0.244
-50	-0.590	-0.584	-0.552	-0.478	-0.316
-55	-0.598	-0.582	-0.558	-0.498	-0.401
-60	-0.602	-0.589	-0.560	-0.504	-0.463
-65	-0.602	-0.591	-0.559	-0.500	-0.469
-70	-0.600	-0.590	-0.555	-0.491	-0.471
-75	-0.597	-0.582	-0.548	-0.475	-0.463
-80	-0.590	-0.572	-0.536	-0.449	-0.444
-85	-0.582	-0.564	-0.523	-0.420	-0.422
-90	-0.576	-0.552	-0.506	-0.382	-0.394

Appendix C: Microprocessor C Code

The following C code was used in the Arduino microcontroller.

```
int leftin = 0;        // select the input pin for the left sensor
int rightin = 1;       // select the input pin for the right sensor
int upin = 2;          // select the input pin for the up sensor
int downin = 3;        // select the input pin for the down sensor
int ref = 5;           // select the amount of hysteresis allowed
int ox1 = 3;           // select the pin for the x axis o1
int ox2 = 4;           // select the pin for the x axis o2
int ox3 = 5;           // select the pin for the x axis o3
int ox4 = 6;           // select the pin for the x axis o4
int oy1 = 12;          // select the pin for the y axis o1
int oy2 = 11;          // select the pin for the y axis o2
int oy3 = 10;          // select the pin for the y axis o3
int oy4 = 9;           // select the pin for the y axis o4
int LV = 0;            // variable to store the left value
int RV = 0;            // variable to store the right value
int DV = 0;            // variable to store the down value
int UV = 0;            // variable to store the up value
int diffx = 0;         // variable to store the x difference
int diffy = 0;         // variable to store the y difference
int Left = 1;          // select the pin for the left LED
int Right = 2;         // select the pin for the right LED
int Down = 7;          // select the pin for the down LED
int Up = 8;            // select the pin for the up LED
int PV = 210;          // select the amount of PWM down time

void setup() {             //Program Setup
  pinMode(ox1, OUTPUT);    //Set pin 3 to output
  pinMode(ox2, OUTPUT);    //Set pin 4 to output
  pinMode(ox3, OUTPUT);    //Set pin 5 to output
  pinMode(ox4, OUTPUT);    //Set pin 6 to output
  pinMode(oy1, OUTPUT);    //Set pin 12 to output
  pinMode(oy2, OUTPUT);    //Set pin 11 to output
  pinMode(oy3, OUTPUT);    //Set pin 10 to output
  pinMode(oy4, OUTPUT);    //Set pin 9 to output
  pinMode(Left, OUTPUT);   //Set pin 1 to output
  pinMode(Right, OUTPUT); //Set pin 2 to output
  pinMode(Up, OUTPUT);     //Set pin 8 to output
  pinMode(Down, OUTPUT);   //Set pin 7 to output
  pinMode(13, OUTPUT);     //Set pin 13 to output
  digitalWrite(13,HIGH);   //Set pin 13 to HIGH to turn on an indicator
LED to show the program is running
}

void loop() {                  //Program Loop
  LV = analogRead(leftin);     //Read the voltage value of the left
sensor to LV
  RV = analogRead(rightin);    //Read the voltage value of the right
sensor to RV
  DV = analogRead(downin);     //Read the voltage value of the down
sensor to DV
```

```
  UV = analogRead(upin);     //Read the voltage value of the up sensor
to UV
  diffx = LV - RV;      //Find the difference between the azimuth
sensors
  diffy = UV - DV;      //Find the difference between the altitude
sensors
  if (diffx > ref)      //If the difference in the azimuth is greater
than the amount specified by ref:
  {
    digitalWrite(ox2, LOW);   //turn off two transistors not being used
    digitalWrite(ox3, HIGH);
    digitalWrite(ox1, HIGH);  //turn on Q1 to allow azimuth motor to
turn left
    analogWrite(ox4, PV);     //Output PWM signal to motor
    digitalWrite(Left, HIGH); //Change indicator LED's to show
    digitalWrite(Right, LOW); //microcontroller sees left as brighter
  }
  else if (diffx < -ref)  //If the difference in the azimuth is less
than the amount specified by the negative ref:
  {
    digitalWrite(ox1, LOW);    //turn off two transistors not being
used
    digitalWrite(ox4, HIGH);
    digitalWrite(ox2, HIGH);   //turn on Q2 to allow azimuth motor to
turn right
    analogWrite(ox3, PV);      //Output PWM signal to motor
    digitalWrite(Right, HIGH); //Change indicator LED's to show
    digitalWrite(Left, LOW);   //microcontroller sees right as brighter
  }
  else                         //If the difference is within the right
amounts
  {
    digitalWrite(ox3, HIGH);   //Turn the low side of the bridge off
    digitalWrite(ox4, HIGH);
    digitalWrite(ox1, HIGH);   //Turn the high side of the bridge on
    digitalWrite(ox2, HIGH);   //to brake the azimuth motor
    digitalWrite(Left, HIGH);  //Set indicator LED's to show that
    digitalWrite(Right, HIGH); //the microcontroller sees both sensors
equal
  }
  if (diffy > ref)
  {
    digitalWrite(oy2, LOW);   //turn off two transistors not being used
    digitalWrite(oy3, HIGH);
    digitalWrite(oy1, HIGH);  //turn on Q1 to allow altitude motor to
turn up
    analogWrite(oy4, PV);     //Output PWM signal to motor
    digitalWrite(Up, HIGH);   //Change indicator LED's to show
    digitalWrite(Down, LOW);  //microcontroller sees up as brighter
  }
  else if (diffy < -ref)
  {
    digitalWrite(oy1, LOW);   //turn off two transistors not being used
    digitalWrite(oy4, HIGH);
    digitalWrite(oy2, HIGH);  //turn on Q2 to allow altitude motor to
turn down
    analogWrite(oy3, PV);     //Output PWM signal to motor
```

```
    digitalWrite(Down, HIGH); //Change indicator LED's to show
    digitalWrite(Up, LOW);    //microcontroller sees down as brighter
  }
  else                        //If the difference is within the right
amounts
  {
    digitalWrite(oy3, HIGH);  //Turn the low side of the bridge off
    digitalWrite(oy4, HIGH);
    digitalWrite(oy1, HIGH);  //Turn the high side of the bridge on
    digitalWrite(oy2, HIGH);  //to brake the azimuth motor
    digitalWrite(Up, HIGH);   //Set indicator LED's to show that
    digitalWrite(Down, HIGH); //the microcontroller sees both sensors
equal
  }
}
```

Appendix D: Microprocessor Schematic

This is the specifications and schematic drawing of the Arduino Duemilanove used in this project, obtained from the manufacturer's website.

Microcontroller:	ATmega328P
Operating Voltage:	5V
Input Voltage (recommended):	7-12V
Input Voltage (limits):	6-20V
Digital I/O Pins:	14 (of which 6 provide PWM output)
Analog Input Pins:	6
DC Current per I/O Pin:	40 mA
DC Current for 3.3V Pin:	50 mA
Flash Memory:	32 KB of which 2 KB used by bootloader
SRAM:	2 KB
EEPROM:	1 KB
Clock Speed:	16 MHz

Schematic on next page

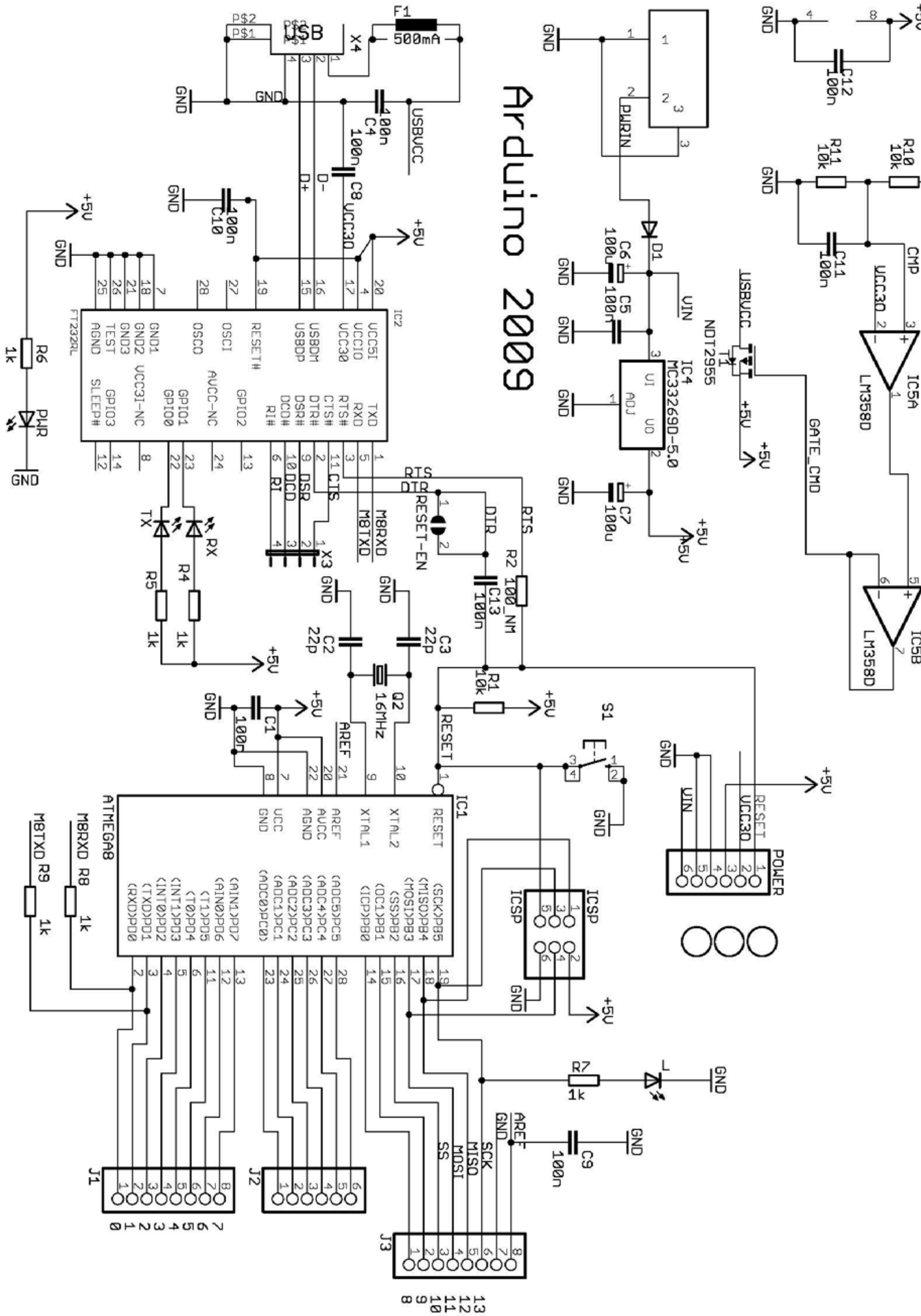
Arduino 2009

Appendix E: MATLAB System Simulation Code

The following MATLAB code was used to simulate the entire system.

```
function mqp (gamma,speed,ref)  %take in values for angle between sensors,
                                %motor speed and comparator reference
                                %gamma is in radians, speed is in rad/s and
                                %ref is in volts
t = 0:0.001:500;       %create a time vector, 500 seconds (500000 ms) long
sun = t*(7.272*10^-5); %create a sun position vector that changes over time
v1 = zeros(1,500001);  %setup a vector for one sensor
v2 = zeros(1,500001);  %setup a vector for the other sensor
pos = zeros(1,500001); %setup a vector for tracker position
n = 2;                 %initialize a indicator
while n <= 500001
    v1(n) = 0.72*cos((gamma/2)-(sun(n)-pos(n-1)))+0.72;
    %current value of v1 is based on angle between sensor and sun which
    %is based on gamma and tracker position
    v2(n) = 0.72*cos((gamma/2)+(sun(n)-pos(n-1)))+0.72;
    %current value of v2 is based on angle between sensor and sun which
    %is based on gamma and tracker position
    if ((v1(n)-v2(n)) > ref)     %if v1 is over the reference and v2 is not
        pos(n) = pos(n-1) + speed/1000;  %rotate towards v1
        n = n + 1;                       %increment indicator
    elseif ((v1(n)-v2(n)) < -ref)%if v2 is over the reference and v1 is not
        pos(n) = pos(n-1) - speed/1000;  %rotate towards v2
        n = n + 1;                       %increment indicator
    else                         %if the difference is between ref and -ref
        pos(n) = pos(n-1);        %do not move
        n = n+1;                  %increment indictor
    end                           %exit if
end                               %exit while
error = (sun-pos)*(180/(pi));   %calculate the error vector between
                                %the sun and tracker

%Plot the sun and tracker movement over 15 seconds:
subplot(2,1,1),plot(t(300001:315000),sun(300001:315000),'black'), hold on,
plot(t(300001:315000),pos(300001:315000),'r'),title('Tracker Movement'),
xlabel('Time (s)'),ylabel('Angular Position (rad)'), hold off;
legend('Sun', 'Tracker');

%Plot the error vector over the same timeframe:
subplot(2,1,2),plot(t(300001:315000),error(300001:315000)),
title('Tracker Error'),xlabel('Time (s)'),ylabel('Error (degrees)');

%Additional Code used to plot voltages on the panels:
%To use, comment out the above plots and uncomment the lines below
%subplot(3,1,1),plot(t(300001:315000), v1(300001:315000)),
%title('Panel 1 Voltages'),xlabel('Time (s)'),ylabel('Voltage (V)');

%subplot(3,1,2),plot(t(300001:315000), v2(300001:315000)),
%title('Panel 2 Voltages'),xlabel('Time (s)'),ylabel('Voltage (V)');

%subplot(3,1,3),plot(t(300001:315000),v1(300001:315000)-v2(300001:315000)),
%title('Difference in Panel Voltages'),xlabel('Time (s)'),
%ylabel('Voltage (V)');
```

Appendix F: MATLAB Power and Energy Simulation Code

The following MATLAB code was used to simulate the power and energy generated over a full year by the four different solar panel setups:

```
function [total DT YT XT NT] = mqpPower (lat,index)
%Take in a latitude in degrees and an index for 1/index points an hour
%Output energy summations for the full year in a row vector

t = 0:(1/index):8760;   %create a time vector 365 days (8760 hours) long
latrad = lat/180*pi;    %translate latitude to radians
w = pi/4380;            %speed of angle to sun in Y (north-south) direction
G = zeros(1,8760*index+1);      %initialize G
Zx = 0.2618.*(t-12);            %angle of sun in X (east-west) direction
Zy = latrad - 0.4102*sin(w.*t); %angle of sun in Y (north-south) direction
I = cos(Zx).*cos(Zy);           %percentage of total radiation possible
ind = find(I >= 0);             %find only when radiation is positive
G(ind) = I(ind);           %create a vector of only positive radiations
tax = 0.9997^2*G;          %dual-axis tracking power percentage
oney = 0.9997*G.*cos(Zx);  %X-axis tracking power percentage
onex = 0.9997*G.*cos(Zy);  %Y-axis tracking power percentage
not = G.*cos(Zy).*cos(Zx); %immobile panel power possible

total = sum(G)/index;    %summation to find energy available
DT = sum(tax)/index;     %summation for energy gained by dual-axis tracking
YT = sum(oney)/index;    %summation for energy gained by Y-axis tracking
XT = sum(onex)/index;    %summation for energy gained by X-axis tracking
NT = sum(not)/index;     %summation for energy gained by immobile panel

%Plot the results over time, comment out for running mqpPower.m:
plot(t(1:25*index),G(1:25*index),'black'),
title('Solar Radiation Absorbed'),xlabel('Time (Hours)'),
ylabel('% Total of Radiation Possible'), hold on, plot(t(1:25*index),
tax(1:25*index),'red'),plot(t(1:25*index),not(1:25*index),'blue'),
plot(t(1:25*index),oney(1:25*index),'green'),plot(t(1:25*index),
onex(1:25*index),'magenta'),hold off;

legend('Sun Radiation','Dual Axis Tracker','Immobile Panel','Y-Axis
Tracking','X-Axis Tracking');

%To Plot over just the first day, put this code in front of all vectors
%in the plot functions:
%(1:25*index)
```

Appendix G: MATLAB Energy Simulation over Latitude Code

The following MATLAB code was used to plot the energy gained by each tracking system over a range of latitudes. It uses mqpPower.m defined in Appendix G.

```
function mqploc
%Function has no inputs

lat = -90:1:90;         %create a latitude vector from 90S to 90N
total = zeros(1,181);   %initialize zero vectors for total sun energy
DT = zeros(1,181);      %initialize zero vectors for all four
YT = zeros(1,181);      %tracking systems
XT = zeros(1,181);
NT = zeros(1,181);

n = 1;                  %initialize an indicator variable
while n <= 181
    [total(n) DT(n) YT(n) XT(n) NT(n)] = mqpPower(lat(n),10);
    n = n+1;
    %cycle through each latitude value and record the energies for
    %all five tracking systems
end %exit while loop

%Plot energy values over latitudes:
plot(lat,total,'black'),title('Energy Generated over Latitude'),
xlabel('Latitude(degrees)'),ylabel('Energy Generated (kWh)'), hold on,
plot(lat,DT,'red'),plot(lat,NT,'blue'),plot(lat,YT,'green'),
plot(lat,XT,'magenta'),hold off;

legend('Sun Radiation','Dual Axis Tracker','Immobile Panel','Y-Axis
Tracking','X-Axis Tracking');
```

Appendix H: Payback Period Data

This Appendix includes the payback period data and calculations done for the immobile system and AADAT system.

	Cost		Energy (kWh)		Price		Payback (Years)	
Solar Panels	Immobile	AADAT	Immob.	AADAT	Immob.	AADAT	Immob.	AADAT
1	108.95	336.16	23.65	35.24	3.62	5.39	30.13	62.39
2	217.90	445.11	47.30	70.48	7.23	10.78	30.13	41.31
3	326.85	554.06	70.96	105.71	10.85	16.16	30.13	34.28
4	435.80	663.01	94.61	140.95	14.47	21.55	30.13	30.76
5	544.75	771.96	118.26	176.19	18.08	26.94	30.13	28.66
6	653.70	880.91	141.91	211.43	21.70	32.33	30.13	27.25
7	762.65	989.86	165.57	246.66	25.32	37.72	30.13	26.25
8	871.60	1098.81	189.22	281.90	28.93	43.10	30.13	25.49
9	980.55	1207.76	212.87	317.14	32.55	48.49	30.13	24.91
10	1089.50	1316.71	236.52	352.38	36.16	53.88	30.13	24.44
11	1198.45	1425.66	260.18	387.62	39.78	59.27	30.13	24.06
12	1307.40	1534.61	283.83	422.85	43.40	64.65	30.13	23.74
13	1416.35	1643.56	307.48	458.09	47.01	70.04	30.13	23.47
14	1525.30	1752.51	331.13	493.33	50.63	75.43	30.13	23.23
15	1634.25	1861.46	354.79	528.57	54.25	80.82	30.13	23.03
16	1743.20	1970.41	378.44	563.80	57.86	86.21	30.13	22.86
17	1852.15	2079.36	402.09	599.04	61.48	91.59	30.13	22.70
18	1961.10	2188.31	425.74	634.28	65.10	96.98	30.13	22.56
19	2070.05	2297.26	449.40	669.52	68.71	102.37	30.13	22.44
20	2179.00	2406.21	473.05	704.76	72.33	107.76	30.13	22.33